*Biochimica et Biophysica Acta*, 1015 (1990) 391–414
Elsevier



BBABIO 43168

# The dynamic aspects of proton transfer processes

Menachem Gutman and Esther Nachliel

*Laser Laboratory for Fast Reactions in Biology, Department of Biochemistry, The George S. Wise Faculty of Life Sciences, Tel Aviv University, Ramat Aviv (Israel)*

(Received 17 July 1989)

Key words: Proton transfer rate; Kinetics; Thermodynamics; Diffusion

## Contents



Correspondence: M. Gutman, Department of Biochemistry, The George S. Wise Faculty of Life Sciences, Tel Aviv University, Ramat Aviv 69978, Israel.

## I. Introduction

The transfer of a proton between adjacent reactants is the most common reaction in the biosphere. Almost all enzymic reactions employ a proton as a reactant, product or intermediate. Furthermore, proton concentration modulates the activity and conformation of all proteins as well as the properties of other macromolecular structures. For this reason in all biochemical textbooks one finds appreciable attention paid to the 'Biochemistry of Protons', but in most cases the treatment is limited to equilibrium parameters. The measurement of the diffusion-controlled kinetics of proton transfer are out of reach of biochemical instrumentation and interest.

The acceptance of Mitchell's chemiosmotic hypothesis introduced a time element to consideration. The flux of proton across active biomembranes must be kinetically competent to account for the measured energy flux (transport, ATP synthesis, redox reactions, flagellar rotation, etc.). The studies aimed in this direction are of quasi-equilibrium systems and are based on steady-state or irreversible thermodynamic formalism. These approximations satisfied the requirement of kinetic competence, but failed to provide a bona fide mechanism of coupling; a mechanism must be proved by a time-resolved, not steady-state kinetics. Thus within the safe boundaries of established thermodynamic measurements and the protective umbrella of insufficient kinetic information, mechanisms of proton transfer-energy coupling models proliferated immune from scrutinizing criticism. In some cases these models were supported by complex physical vocabulary which, though impressive, was sometimes irrelevant. For this reason we shall provide in this manuscript a clear physical description of the mechanism of proton transfer.

Clarification of physical terminology is not a goal in itself, yet it is instrumental for the elucidation of the information obtainable from proton transfer measurements. The currently accumulated theories on the rates of proton transfer and its diffusion are suitable to derive specific information about the environment where the reaction takes place. Thus, parameters like activity of water, density of immobile binding sites, viscosity of the solvent or electrostatic interaction can be measured.

With such opportunities at hand, the advantage of a short observation period is self-evident. If we can limit the monitoring to a very short time frame, after a proton has been released in a defined site, the physical information obtained by the analysis will reflect only that space which the proton could probe during the observation time. Thus the temporal resolution is transformed into spatial resolution. Under proper conditions, microspace as small as the hydration layer of a protein or the specific site on a protein can be studied, totally insensitive to the huge bulk volume in which the sample is suspended.

The time-resolved study of proton transfer has been measured in a few enzymatic systems, such as bacteriorhodopsin, the photosynthetic reaction centre and some redox enzymes. There is no advantage in our reviewing these studies. At most, we should be able to redescribe or co-interpret the observation of the original authors. What we wish to do is to spread a framework of general conclusions about the proton transfer phenomenon. Section II of this review describes the main factors which govern the rate of proton transfer and diffusion in aqueous solutions. Section III implements this knowledge for evaluation of reactions taking place in the heterogeneous matrix of a protein and membrane surface.

It is our conviction that this information will be instrumental both for specific analysis of future experiments and, equally important, for formulation of a strong intuitive concept of what are the permissible scenarios for proton-coupled energy transformation in bioenergetics.

## II. Mechanism of proton transfer

### *II-A. Spatial and temporal characteristics of proton transfer*

#### *II-A.1. The effect of relative orientation of donor-acceptor in a hydrogen-bonded pair*

In aqueous solution, reactants interact with the solvent molecules about $10^{15}$ times per second. Obviously in such a dynamic matrix the distance and relative alignment between potential proton donor-acceptor pairs will vary rapidly. Whatever we measure under such conditions is an average over all possible positions. In comparison, proteins are rigid glassy matrices in which the relative motion of amino-acid chains is severely restricted. In such a semi-immobilized environment, minor realignment of amino-acid side-chains may affect the distribution of proton between the two possible locations as well as the energy barrier of the transfer.

Experimentally it is impossible to carry out a controlled measurement in which two molecules are fixed in space and the proton is exchanged between them. Theoretical ab initio molecular orbital calculations, as carried out by Scheiner, are not subject to this experimental problem; the geometry of the donor-acceptor pair is given as fixed coordinates, while the energy of the proton is systematically calculated over the whole space. The results of such computations are expressed as a map of the energy difference ($\delta E$) associated with the transfer of the proton between the two locations and the activation energy ($\delta E^*$) needed for this transfer [1].

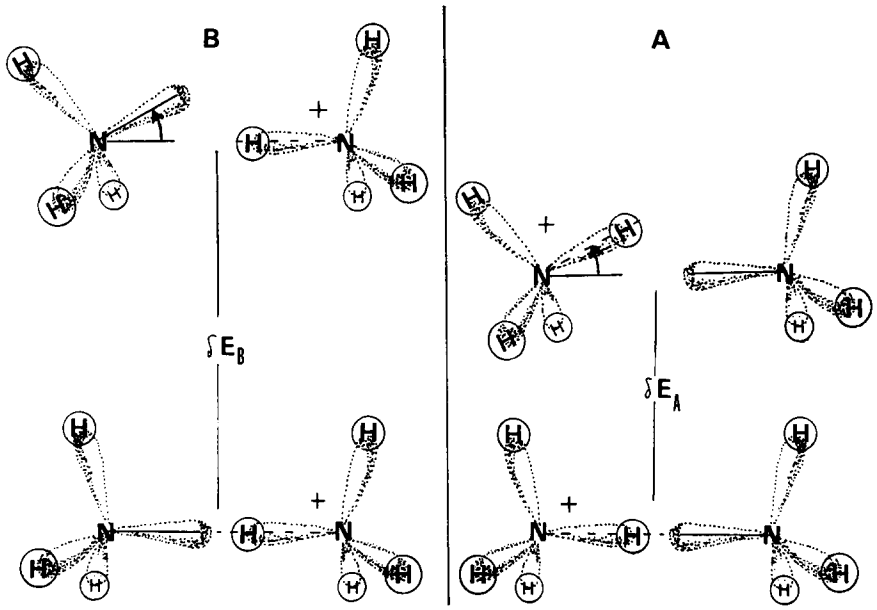


Scheme I. Schematic diagram of equilibrium configurations of two $NH_3$ molecules hydorgen-bonded by a single proton. The bottom configurations are equipotential symmetric structures where the proton is located on the N–N axis. The upper configuration results from a rotating left-hand molecule with respect to the N–N axis. The energy needed to rotate the $NH_4^+$ molecule in the A configuration ($\delta E_A$) is smaller than that needed to rotate the $NH_3$ molecule as in the B configuration ($\delta E_B$). That is because the rotation of $NH_4^+$ does not perturb the charge–dipole interaction. The left-hand configuration has lost this stabilization as the dipole does not point towards the charge. For more detials see Scheiner [1].

The most illustrative example is given in Scheme I, where two $NH_3$ molecules exchange a proton between them. When the two lone pairs of the nitrogen atoms point towards the proton located between them, the system is symmetric and the proton can assume, with equal probability, either the left or the right position. In both configurations the dipole moment of one $NH_3$ is pointing towards the positive charge of the $NH_4^+$. The situation changes if the left-hand $NH_3$ group is rotated so that its dipole vector is turned away from the N–N axis. In that case the two locations of the protons are not of equal energy. Locating the $H^+$ on the left-hand molecule will still gain stabilization by dipole (right)–charge (left) interaction (A). The proton on the right-hand $NH_3$ will be less stable, as the dipole vector does not point to the charge (B). This difference varies with the angle of alignment and can be as high as 2.5 kcal/mol, i.e., the geometry has imposed a $\Delta pK \approx 2$ between the two identical groups [2]. The same considerations apply for proton transfer between water molecules, carboxylic acids or amino groups. The $\delta E$ values imposed by an unfavourable alignment can amount to about 10 kcal/mol (Ref. 3 and references therein).

If we now apply these conclusions to the reality of amino-acid side-chains, we can visualize 'proton rectifier' configurations; the restricted motion of hydrogen-coupled pairs will favour a directional proton transfer.

The distance between the proton-exchanging pair has a marked effect on the activation energy. Most hydrogen-bonded systems maintain a 2.7–2.3 Å distance between the nuclei. As the distance increases, the energy barrier of the proton transfer increases, with a slope of about 30–60 kcal/mol per Å. Thus, the distance be-

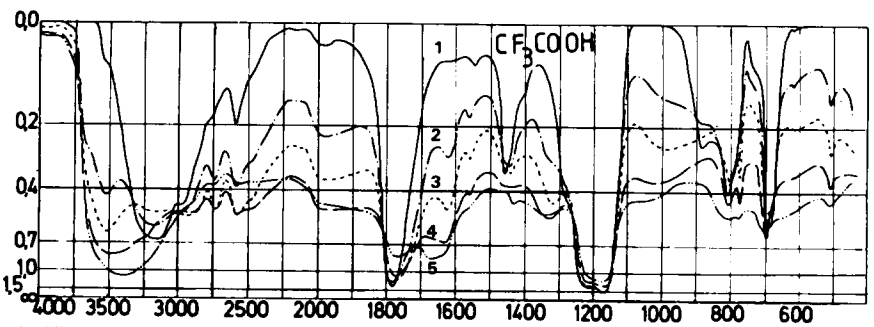


Fig. 1. Infrared spectrum of trifluoroacetic acid as measured with increasing water content. The mole ratio (acid/water) increases in curves 1 to 5 from 0 to 0.42; 0.88; 2.0 and 5.1, respectively. Note how the discrete bands are lost and the gaps between them are filled with the continuum absorbance. Figure taken from Leuchas and Zundel [6].

tween a properly aligned pair in a protein can function as a proton switch which shifts the system from conductive to disengaged position with a sliding motion of 1–2 Å. The electric field also regulates the probability and activation energy of proton distribution between two sites [4]. Placing a positive or negative charge near one group of a hydrogen-bonded pair will shift the favourable position of the proton and lower the activation energy of the process.

*II-A.2. Time-averaged measurements of proton transfer within hydrogen-bonded pairs*

Under the influence of external electric field the proton involved in hydrogen bonding will shift its position between the two energetic minima of the potential field. The frequency of the transition is controlled both by the energy difference between the minima ($\delta E$) and the height of the energy barrier ($\delta E^*$). In the case that either of these is high, the proton will be arrested in one place due to thermodynamic (high $\delta E$) or kinetic (high $\delta E^*$) restraints. If the two hydrogen-bonded nuclei are sufficiently close for the two energy minima to merge, the proton will move freely between the two sites, forming a state of high polarizability which is readily detected by infrared spectroscopy [5]. The oscillating electric field of the infrared photons interact with those hydrogen-bonded pairs which, as determined by their momentary distance and alignment, match their proton exchange frequency with that of the photon. As pointed out by Zundel, each photoselective proton transfer as a discrete wavelength, but, due to the widespread population of $\delta E$ and $\delta E^*$, the proton transfer infrared absorption will be a broad featureless band, defined as continuum absorbance.

A typical absorption spectrum is shown in Fig. 1. The uppermost line is the infrared spectrum of anhydrous trifluoroacetic acid, where the various vibration bands are clearly observed. Addition of increasing amounts of water (0.42, 0.88, 2.0 and 5.1 molecules per acid) fills up the gaps between the absorption bands to an almost featureless spectrum. This continuum absorbance represents the accumulation of COOH-$H_2O$ structures which, due to microscopic dynamic heterogeneity, merge their discrete bands. On further dilution, when the acid is totally dissociated, the intensity of the continuum absorbance diminishes [6].

The continuum infrared absorbance was measured in many systems with high polarizability due to hydrogen bonding as in the following examples: a mixture of poly(L-glutamate)-poly(L-lysine) slightly wetted (90% humidity) to provide a water molecule to bridge between donor and acceptor; proton exchange between the carboxylic acid and phospho moiety of phosphatidylserine [7] and/or in aqueous solution of high charge density cations (like $Li^+$) which depolarize the solvating

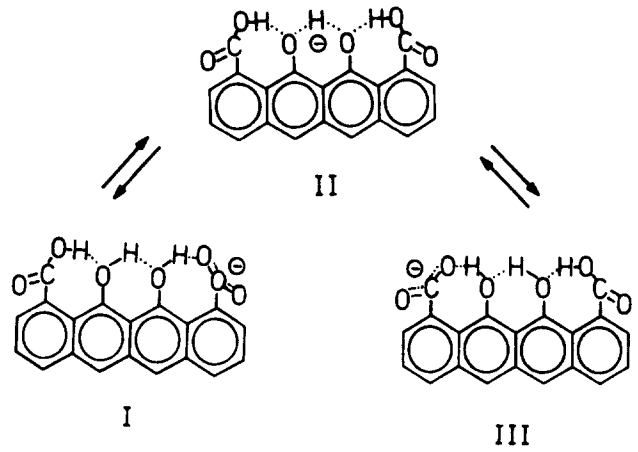


Scheme II.

water molecules to form [$Li^+$, $OH^- \cdots H^+ \cdot H_2O$] structures [8].

The capacity of multi-potential minima structures to function as extended proton transfer structures is a commonly adopted concept [9,10]. According to these models, an array of ordered sites like OH or carboxylic acids rapidly transport protons across [9] or along [10] the surface of the membrane. These models are experimentally approximated by structures like 11,12-dihydroxy-1,10-naphthacenedicarboxylic acid (Scheme II). The proton in this compound is highly polarizable, with a typical clear continuum absorbance [11]. A salient point in this study is the required rigidity of the multiminima structure. The rigid polyaromatic structure is crucial in maintaining the central phenol oxygens in a constant position, ensuring the formation of a broad potential minimum at the centre of the molecule. The same criterion must be applied for evaluation of the models of Nagel and Morowitz [9] or Haines [10]. The proposed conductive structures must be sufficiently stable not to lose their rigidity by thermal fluctuations.

The time frame of proton transfer in highly polarizable proton array is comparable with the time frame of the vibration and stretching transition of the building blocks of the array, i.e., $(10–50) \cdot 10^{-15}$ s. This implies that not only nano- and picosecond events will determine the efficiency of proton transfer – to a large extent the femtosecond fluctuation of the hydrogen bonded structure will determine the efficiency of the process. To evaluate quantitatively the capacity of complex structure to conduct a proton, one must resort to molecular dynamic calculation where both energetics and molecular motion are combined.

*II-A.3. Molecular dynamic simulations of proton transfer*

Molecular dynamics simulate the fluctuations of atoms over a time frame of a few picoseconds at femtosecond intervals. At each time point the position and potential of all atoms are calculated, accounting for

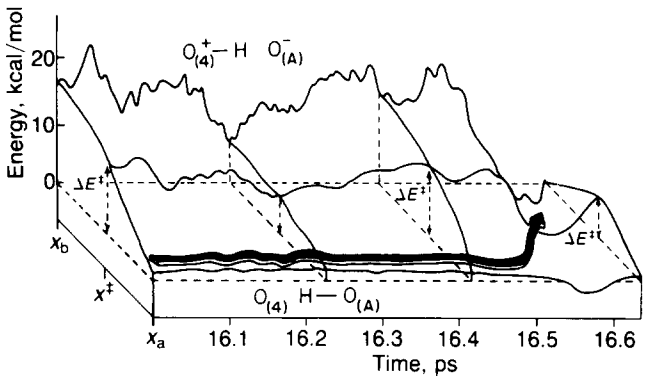


Fig 2. Time-dependent variation of the energy of a proton along the axis between the glutamate-35 oxygen and the $O_{(4)}$ oxygen of a substrate bound to the active site of lysosyme. The energy is drawn as it varies with position and with time, due to random fluctuations of protein and solvent molecules. At $t \approx 16.5$ ps the energy barrier ($\Delta E^{\ddagger}$) at the mid-point ($X^{\ddagger}$) between glutamate ($X_a$) and acceptor ($X_b$) is momentarily lowered and proton transfer (black arrow) takes place. The calculation and figure are by A. Warshel [12].

random thermal fluctuations, as well as for short and long range forces. Through these calculations the trajectory of group translocation is envisioned as an occasional situation where the energy barrier separating the donor and acceptor potential wells is temporarily lowered by favouring random combination of forces applied by neighbouring atoms. These computations are carried out for well-defined structures like proteins and enzyme-substrate complexes, where all atom coordinates are known.

A typical proton transfer trajectory, calculated by Warshel, is given in Fig. 2. It depicts the transfer of proton from glutamate-35 of lysosyme to the oxygen atom of a substrate held in the active site [12]. The foreward abscissa ($X_a$) depicts the variation with time of the energy of a proton covalently attached to the glutamate's carboxylate. The potential of the proton in this position is determined by the covalent bonding resonance and the electrostatic energy. The backward abscissa ($X_b$) depicts the energy of a proton when bound to the oxygen of the sugar (oxonium). The energy is determined by the ionic resonance and electrostatic stabilization of the oxonium by the charges and dipoles of the surrounding protein and solvent molecules. Because of the ionic nature of the product, its potential is more sensitive to the electrostatic term fluctuation and generally is less stable than the donor site.

At a certain time ($\approx$ 16.5 ps), the random fluctuation of charges and dipoles generates a transient configuration which makes the oxonium state more stable than the carboxylic acid. This configuration also lowers the potential of the transition state ($X^{\ddagger}$ in the figure), where the energy is affected by the resonance and electric potential of the donor and acceptor configuration. The potential-energy gradient ($dE/dx$) is a force which propels the proton at a velocity of about $10^{13}$ Å/s along the reaction coordinate and the proton transfer is established. As the proton transfer itself is so fast, the rate-limiting step of the overall event is the waiting period in which the proton is energetically and kinetically confined to one configuration. This provides us with an intuitive understanding of the rate constant of proton transfer reactions. It is the reciprocal of the waiting period during which donor-acceptor and solvent molecules fluctuate at random until the favourable configuration is attained. (This rate constant is of the chemical reaction per se and is not to be confused with the rate of encounter between the reactants during their random diffusion in the solution; see II-C.2, below.)

The time frame of the proton transfer per se, a few femtoseconds, is comparable with the frequency of the infrared resonance of highly polarizable hydrogen bonds. Within such a short time the molecules are practically frozen in space. This leads to an obvious restriction on all proton transfer reactions; in no case will a proton leave the donor site unless the acceptor 'nest' is ready.

Dissociation of an acid in aqueous solution is a proton transfer from the acid to water molecules acting as an acceptor. The rotation of water molecules ($\approx$ 10 ps) is orders of magnitude slower than proton transfer, and hydration of proton by a single water molecule is not sufficient to stabilize it. Thus, hydrative stabilization of the proton should be a highly cooperative event; few water molecules must be in a favourable acceptor configuration to catch the dissociating proton.

The cooperativity (with respect to water) was experimentally detected by Gutman and his colleagues [13,14] and confirmed by Bardez et al. [15], Shizuka et al. [16] and Politi and Chaimovich [17]. In these time-resolved measurements, proton dissociation was synchronized by a picosecond laser flash which excited a hydroxy-aromatic compound to excited singlet state, in which the hydroxyl proton becomes very acidic. The excited species dissociation is much longer than the few femtoseconds of the actual step of hopping over the barrier. Thus we can ascribe it to the 'waiting for the proper opportunity' period.

When the activity of water in the solution is lowered by addition of strong electrolytes, the rate of dissociation becomes much lower (see Fig. 3), following an empirical relation:

$$k_1 = k_0 (a_{H_2O})^n \qquad (1)$$

where $n$ varies between 6 and 10 depending on the dissociating acid, not on the nature of compound used for changing $a_{H_2O}$.

The slower dissociation with decreased water activity represents the modulation of the rate-limiting step of proton dissociation by the scarcity of acceptor sites in the solution.

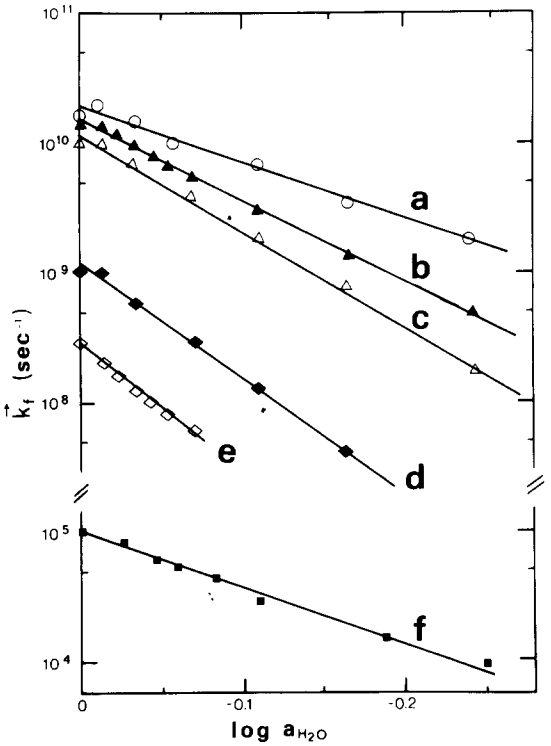


Fig. 3. The dependence of the rate of proton dissociation from an acid on the water activity of the solution. The rates were measured by time-resolved kinetics as described in Ref. 14. The acidic groups are: (a) 2-naphthol 3,6-disulphonate (excited state); (b) 2-naphthol 6,8-disulphonate (excited state); (c) 8-hydroxypyrene 1,3,6-trisulphonate (excited state); (d) 2-naphthol 6-sulphonate (excited state); (e) 2-naphthol (excited state); (f) Bromocresol green (ground state). Note discontinuity of the ordinate.

As shall be detailed below, these kinetic measurements are extremely useful for monitoring the activity of water in specific sites such as defined cavities in proteins [13,18] or the inner aqueous phase of reversed micelles [15,17].

### *II-B. Diffusion of proton in aqueous solutions*

#### *II-B.1. Diffusion in liquid water*

Water is a peculiar liquid. At room temperature each water molecule maintains an average of about 2.6 hydrogen bonds with its immediate neighbours located at a distance of 2.75 Å (oxygen–oxygen). Such a level of connectivity suffices to establish a continuous percolating network of hydrogen-bonded water molecules extending through the whole volume of any body of water [19]. The short lifespan of the hydrogen bond, $\tau_{HB} = 2.3$ ps, gives the percolating network tremendous flexibility: within 1 mol of water molecules $2.6 \cdot 10^{35}$ hydrogen bonds are dissolved and reestablished within each second.

The dynamic network of hydrogen-bonded water molecules is an excellent path for proton transfer reactions. Within the 2.3 ps that two water molecules are hydrogen bonded, their distance and alignment are perfect for proton transfers, an event which takes about 45 fs [20].

The dynamic network readily incorporates and interconnects with the hydrogen-bonded proton hydrate ($H_9O_4^+$) (or even larger structures). Thus, propagation of $H^+$ (also $OH^-$) in water differs from all other solutes. It is a translocation 'by proxy' and not a self-diffusion. Indeed, the diffusion coefficient of proton in water, $D_{H^+} = 9.28 \cdot 10^{-5}$ cm$^2 \cdot$ s$^{-1}$ (25 °C), is about 3-times larger than the self-diffusion of $H_2O$ in the same matrix, $D_{H_2O} = 2.8 \cdot 10^{-5}$ cm$^2 \cdot$ s$^{-1}$ (25 °C). The percolating network of the water molecules which paves the way for the proton restrains the self-diffusion of its structural elements [19].

Propagation of proton in matrix of hydrogen-bonded water molecules is encountered also on surface of proteins [21]. The dielectric constant of dry protein is low. When proteins are slightly wetted, their dielectric constant increases due to rapid proton translocation mediated by the adsorbed water molecule. The amount of coverage of the surface needed for the change in surface proton conductivity is $40 \pm 4\%$ of total surface sites. This value is very close to the theoretical predicted value $45 \pm 3\%$ of coverage by interconnecting elements needed to establish long-range connectivity on a surface.

The capacity of the percolating network to conduct protons over microscopic stretches of about 30 Å was demonstrated experimentally by breaking the connectivity through addition of organic solvents to water [22]. The addition of solvents like methanol, ethanol or propanol to an aqueous solution of pyranin (8-hydroxypyrene 1,3,6-trisulfonate) delays the observed dissociation of proton from the excited molecule. The measured rate of dissociation in the presence of the alcohols is lower than that predicted by the activity of water in the solution.

The interpretation of this observation hinges on the disruption of the percolating network of hydrogen-bonded water by the organic solute. As a result, the escape of the proton from the Coulomb cage is delayed and accordingly the probability of recombination increases (see below, section II-C.2b).

#### *II-B.2. The effect of (non) random structures on proton diffusion*

Highly ordered water molecules, stabilized by hydrogen bonding, provide a favoured structure for propagation of proton. This argument apparently suports the common notion that proton diffusion in ice is faster than in liquid water by 1 to 2 orders of magnitude. At present there are strong experimental and theoretical objections to this notion (Ref. 23, and many other articles in this book). Time-resolved measurements of proton diffusion in ice and supercooled water reveal a

clear difference between the two matrices [24]. In ice $D_{H^+} = 0.7 \cdot 10^{-5}$ cm$^2 \cdot$ s$^{-1}$, while in water (both at $-10\,^\circ$C) $D_{H^+} = 4.1 \cdot 10^{-5}$ cm$^2 \cdot$ s$^{-1}$.

As proton is transferred from a donor water molecule [$H_2OH^+$] to the acceptor one along the hydrogen bond it leaves a wake behind it: the unpaired electronic orbital which points towards the acceptor. Thus the net electric charge transported is not a full protonic charge: 36% of it is neutralized by the unpaired orbital [24]. The resulting ionic defect in the structure can relax by two mechanisms; the donor pair will rotate, and by randomization will make the transfer permanent full charge transition, otherwise the proton will relax to its original position, returning to the donor molecule. Thus, a proton moving along an ordered rigid water molecule structure will leave behind a trail of oritneted electric vectors pointing in the direction of its motion. In the absence of relaxational rotation, which is hindered in ice-like crystal, the proton will never 'forget' the way it came and may return by the same route. It is the impermanence of structure in liquid water which makes the proton so diffusive. The short life-span of the hydrogen bond, $\tau_{HB} = 2.3$ ps, introduces the randomization of the proton passage, which is the fundamental property of a diffusive process.

A random walk process is associated with a diffusion coefficient, $D = \nu d^2/6$, where $\nu$ is the frequency at which a particle makes a random irreversible step with a length of $d$. If proton diffusion in liquid water is through the percolating network of hydrogen-bonded molecules, then the step length will be that of a hydrogen bond ($d = 2.75$ Å) and $\nu$ will be the frequency of random irreversible step events. Using this expression we obtain $\nu^{-1} = 1.3$ ps, which is in very good agreement with the lifetime of the hydrogen bond, $\tau_{HB} = 2.3$ ps. The pace maker frequency is thus the randomization rate at which the percolating network is changing its connectivity.

Based on this conclusion we can generalize that, in a microenvironment where prevailing forces enhance a less flexible hydrogen-bonded network (such as the hydration water of membranes or proteins), the diffusion coefficient in this space will be smaller than in bulk water, while exchange of proton between two nearby sites will be faster. There is no contradiction between these two predictions; they are a reflection of the same mechanism.

### *II-C. Rates and velocities of proton transfer reactions*

*II-C.1a. Rate of dissociation.* Proton dissociation is actually its transfer from the acidic moiety (AH) to water. Under conditions where the acceptor availability is not rate-limiting ($a_{H_2O} = 1$) (see Fig. 3), the rate is controlled by the thermodynamic stability of HA. A reversible one-step dissociation will fit a simple relationship between the rate constant and the thermodynamic constant

$$k_d = k_a \cdot K_d \tag{2}$$

As in most cases the binding of proton ($k_a$) is diffusion controlled reaction, its value will vary over a rather narrow range. Consequently, the rate constant of proton dissociation will be directly proportional to the p$K$.

Fig. 4 is a compilation of rate constants of proton dissociation, measured by time-resolved fast-kinetic experiments. The accuracy of these rates is about 20% or better. We find that small solutes as well as surface groups of proteins and phospholipids (carboxyls, amino groups, histidine residues, nitrotyrosin, phospho moieties, covalently bound fluoresceins or adsorbed dyes) all fit a single straight line.

The deviations from the line are small and in most cases directly related to the allowable range of $k_a$ value (see below). This strict correlation between the rate constant and equilibrium constant classifies these reactions as reversible one-step binding. A compound or reaction which deviates from this simple relationship implies that the discharge of the proton is controlled by another step preceding the actual transfer to the water.

*II-C.1b. Rate of hydrolysis.* Kasianowicz et al. [25] measured the rate at which the ionophore S-13 transports protons across a black-lipid membrane. Their results indicated that, besides direct protonation of the uncoupler by free protons, there is a substantial protonation by hydrolytic reaction on the membrane's surface.

Hydrolysis, which makes the water an inexhaustible source of protons, can be a rather slow reaction. Basically, it is a reversible reaction which in one direction (forwards) is an abstraction of proton from water molecule by a base ($A^-$), while the backward reaction is a diffusion controlled neutralization of the conjugate acid by $OH^-$.

$$A^- + H_2O \underset{k_n}{\overset{k_{hy}}{\rightleftharpoons}} AH + OH^-$$

The rate constant of the hydrolytic event is expressed as proceeding in 55.5 M $H_2O$ and is given by

$$k_{hy} = k_n \cdot 10^{(pK - 15.74)} \tag{3}$$

The velocity of the reaction is thus dependent on the difference in stability of two compounds AH and $H_2O$ as expressed by the exponential term ($k_n$ is almost constant and its magnitude is diffusion controlled).

The rate of hydrolysis is sensitive to the reactivity of the water. It can be increased by the polarization of the water molecule by the strong electric field of a small cation (Gutman and colleagues [26]). Heterocyclic

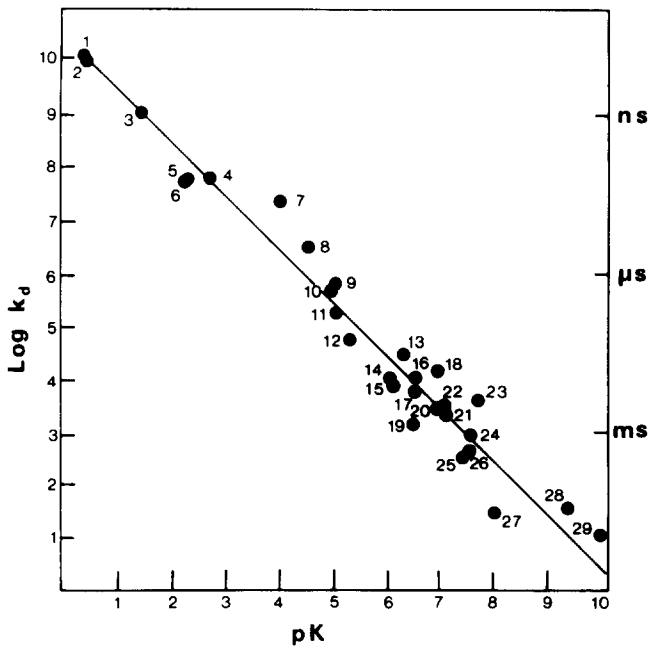


Fig. 4. Correlation between the rate constant of proton dissociation and the p$K$ of the acid. All values were measured by the Laser Induced Proton Pulse [47,48] in dilute solutions where $a_{H_2O} = 1$. The rate constants were derived from the time-resolved measurements by numerical simulation of the kinetics (for details see Refs. 47, 48). The compounds studied are as follows:

(1) pyranin (excited state);
(2) 2-naphthol 3,6-disulphonate (excited state);
(3) 2-naphthol 6-sulphonate (excited state);
(4) 2-naphthol (excited state);
(5) phosphatidylcholine;
(6) phosphatidic acid (low p$K$ ionization);
(7) carboxylates of RNase (average for all groups);
(8) carboxylic acid of phosphatidylserine;
(9) carboxylates of bovine serum albumin (average);
(10) Bromocresol green;
(11) 6-methoxyquinolinium;
(12) acridinium;
(13) Bromocresol purple;
(14) glutamate-35 of lysosyme;
(15) Mes;
(16) fluorescein adduct to α-amino of RNase;
(17) fluorescein adduct to bovine serum albumin;
(18) Bromothymol blue;
(19) histidine of RNase;
(20) imidazole;
(21) nitrotyrosine of lysosyme (average);
(22) fluorescein;
(23) pyranin (ground state);
(24) 7-hydroxycumarine;
(25) α-amino of lysosyme;
(26) *ortho*-nitrophenol;
(27) phosphatidic acid (high p$K$ ionization);
(28) 2-naphthol (ground state);
(29) ε-amino of lysine in bovine serum albumin (average).

aromatic compounds like acridine or quinoline derivatives, when excited to their first electronic singlet state, become very strong bases (p$K^*$ ≈ 11 [27]). The excited base reacts rapidly with the water, forming $\phi N^*\text{-}H^+$ within the lifetime of the excited state.

The rate of this reaction can be accelerated up to 1000-fold if the proton donor molecule is bound to a high charge density cation such as $Mg^{2+}$ [26].

On the basis of these measurements we conclude that the capacity of water to supply protons for fast catalytic reactions (with turnover number of 1000/s or more) will be met only if the p$K$ of the active site is higher than 8. In the presence of strong polarizing cation the rate of hydrolysis by the same group may be faster.

*II-C.2. Rate constants of proton binding*

*II-C.2a. Diffusion-controlled reactions.* The rates of protonation of many compounds are compiled in Table I. As seen in this table, the rate constants of proton binding either to small solutes or to surface groups of a large macroscopic structure (planar black lipid membrane) fall in a rather narrow range, $10^{10}$–$10^{11}$ $M^{-1} \cdot s^{-1}$. The high accuracy at which these rate constants can be measured (±20% or less) made them suitable for quantitative analysis through the Debye-Smoluchowski equation

$$k_{AB} = \frac{4\pi N R_0 \Sigma D}{1000} \cdot \frac{\delta}{e^{\delta} - 1} \cdot e^{\delta(r_0\kappa/(1+r_0\kappa))} \qquad (4)$$

In this equation $N$ is Avogadro's number. The reaction radius, $R_0$, is how close proton can approach before a covalent bond is formed (6–7 Å in most cases). $\Sigma D$ is the sum of the diffusion coefficients, but, due to the rapid diffusion of $H^+$, we can approximate $\Sigma D \cong D_{H^+}$.

The product of these numbers is the rate of encounter between the two species as determined by their diffusion in the solution, $k_{en} \approx 4 \cdot 10^{10}$ $M^{-1} \cdot s^{-1}$.

The second term in the equation, $\delta/(e^{\delta} - 1)$, represents the contribution of the electrostatic potential in infinitely dilute solution ($I = 0$). The value $\delta$ is the ratio between the size of the Debye radius, $R_D$, and the radius of reaction, $\delta = R_D/R_0$. $R_D$ is defined as the distance at which the electrostatic potential is equal to the thermal energy:

$$R_D = Z_1 Z_e e_0^2/\varepsilon kT$$

By definition $R_D$ is always positive. In aqueous solution at room temperature $R_D = 7 \cdot (Z_1 Z_2)$ (given already in ångström units). It should be noted that when the dielectric constant of the solution decreases, for example in concentrated sucrose solution or in presence of organic solvents, $R_D$ increases.

Unlike $R_D$, which is positive, $\delta$ has the sign of the charge product, $Z_1 Z_2$, and reflects whether a proton within the distance $R_D$ will be attracted to the anion or repelled by cation. Thus, for $Z_1 Z_2 < 0$, the expression $\delta/(e^{\delta} - 1) > 1$, while for repulsion ($Z_1 Z_2 > 0$) the term is smaller than 1.

TABLE I

*Diffusion-controlled second-order rate constants of protonation as determined by the Laser-Induced Proton Pulse*

| Compound | $k$ ($10^{10}$ $M^{-1}\cdot s^{-1}$) | Ref. |
|---|---|---|
| (1) Rate constants of protonation of ground-state proton emitters | | |
| 8-hydroxypyrene 1,3,6-trisulphonate | 18 ±1.5 | 47 |
| 2-Naphthol 3,6-disulphonate | 7 ±0.5 | 47 |
| 2-Naphthol 6-sulphonate | 7.6 ±0.4 | 47 |
| 2-Naphthol | 1.0 ±0.1 | 47 |
| 7-Hydroxycoumarin | 4.5 ±0.5 | 47 |
| 6-Methoxyquinolin | 2.0 ±0.15 | 27 |
| Acridine | 1.0 ±0.1 | 27 |
| (2) Rate constants of protonation of indicators | | |
| Bromocresol green | 4.2 ±0.1 | 47 |
| Bromothymol blue | 4.5 ±0.1 | 27 |
| Fluorescein | 2.0 ±0.5 | 47 |
| *o*-Nitrophenol | 3.0 ±1.0 | 84 |
| (3) Rate constants of protonation of buffers | | |
| Imidazole | 2.0 ±0.1 | 47 |
| Mes | 1.0 ±0.3 | 51 |
| (4) Rate constants of protonation of surface groups | | |
| A. Adsorbed indicators | | |
| Bromocresol green on Brij-58 | 0.65 ±0.05 | 47 |
| Neutral red on Brij-58 | 0.9 ±0.03 | 47 |
| Bromocresol green on PC liposome | 2.5 ±0.2 | 57 |
| Bromocresol green on PC-cholesterol liposome | 2.7 ±0.2 | 57 |
| B. Covalently attached groups | | |
| Fluorescein on BSA | 2.5 ±1.5 | 59 |
| Fluorescein on RNase | 3.0 ±0.25 | 84 |
| Nitrotyrosine of lysozyme | 2.0 ±0.5 | 84 |
| $COO^-$ of BSA | 2.5 ±0.6 | 59 |
| $COO^-$ of RNase | 2.5 ±0.25 | 84 |
| $COO^-$ of lysosyme | 1.2 ±0.1 | 84 |
| Glu-35 of lysosyme | 1.2 ±0.1 | 84 |
| His of RNase | 0.5 ±0.1 | 84 |
| α-Amino of lysosyme | 1.0 ±0.1 | 84 |
| Lys of BSA (average) | 0.5 ±0.25 | 59 |
| Lys of lysosyme (average) | 0.5 ±0.25 | 84 |
| C. Phospholipid headgroups | | |
| Phosphatidylcholine | 0.6 ±0.1 | 57 |
| Phosphatidylserine | 1.5 ±0.25 | 57 |
| Phosphatidic acid ($A^-$) | 0.75 ±0.25 | 57 |
| ($A^{2-}$) | 0.35 ±0.25 | 57 |

The last term in Eqn. 4 is a correction for the electrostatic screening where $\kappa = 3.3 \cdot 10^7 \cdot \sqrt{I}$ ($cm^{-1}$).

At low ionic strength the last term is approx. 1 and the full electrostatic force affects the rate of the reaction. At high ionic strength ($I \approx 1$) the product of the two electrostatic terms is close to 1 and $k_{dc} \simeq k_{en}$.

The applicability of Eqn. 4 for calculation of diffusion coefficient of a proton-anion pair was demonstrated by Pines and Huppert [28]. At present it is a useful tool for calculating the diffusion coefficient of proton in microscopic spaces where no other method can be employed [29].

*II-C.2b. Proton–anion geminate recombination.* The Debye-Smoluchowski equation (Eqn. 4) describes the mutual search of the reactants until the distance between them is $r = R_D$. Once the proton sinks below the surface of the sphere limited by the Debye radius, also referred to as the Coulomb cage, the rate of events is highly accelerated by the strong electrostatic attraction. Within a fraction of a nanosecond the proton will approach to the distance of contact ($R_0$) and the actual chemical reaction, formation of a covalent bond, will take place. In comparison to the long mutual search, the events within the Coulomb cage are rapid and are therefore ignored.

The electric forces are of major importance in ionic dissociation. The proton-anion pair is formed at a contact distance and the two species attract each other electrostatically. The separation of the pair is the diffusion of the proton against the electric field. As long as the proton is within the Coulomb cage its random diffusion is biased. Consequently, a strong electric field will increase the probability that the pair will approach the contact radius, and the covalent bond may be renewed. The process whereby ions separate and recombine before the distance exceeds $R_D$ is called 'geminate recombination'.

The probability that a proton will eventually emerge out of an attractive Coulomb cage is approximated by $P_{escape} = \exp(-R_D/R_0)$. This probability term reduces the fraction of free protons in the solution, and experimentally it is incorporated in the measured p$K$. For a detailed discussion of the relation between the measured $K_d$ and geminate recombination, see Agmon [30] and references cited therein.

The time frame in which geminate recombination takes place is extremely short. Within a few nanoseconds the final equilibrium of free ions is established. Experiments carried out within this time-scale, such as reaction of excited molecules, must consider geminate recombination. In the last decade, the usage of fluorophores for measuring intracellular and intraorganelle pH has expanded [31–34] without consideration that the lifetime of the excited state falls within the time frame of geminate recombination. Such negligence should be avoided.

$$AH \underset{k_r}{\overset{k_d}{\rightleftarrows}} [A^- \text{------} H^+] \rightleftarrows A^- + H^+$$

Scheme III.

The reactions which we must consider are defined in Scheme III. The covalent bond A–H is broken and reformed with rate constants $k_d$ and $k_r$, respectively, producing consuming a proton at a contact distance $r = R_0$. From this starting position the proton diffuses

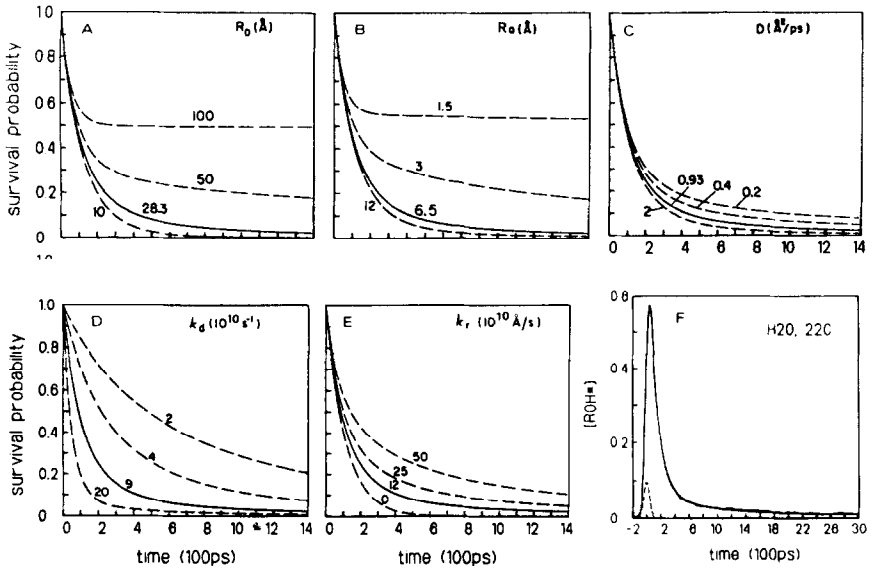


Fig. 5. Simulated dynamics of geminate recombination between proton and anion. In each frame the survival probability of the acidic state is drawn vs. time, as it varies by one adjustable parameter. The continuous line is that which best corresponds with the excited pyranin dissociation. (A) The effect of electrostatic field, given as a Debye radius ($R_D$). (B) The effect of contact radius ($R_0$). (C) The effect of the diffusion coefficient of proton in water ($D_{H+}$). (D) The effect of the rate of covalent bond breaking ($k_d$). (E) The effect of rate of covalent bond formation ($k_r$) at a distance of $r = R_0$. (F) Complete reconstruction of pyranin dissociation kinetics by the rate constants corresponding with the heavy lines in frames A–E. The reconstruction is over a 30 ns observation time, i.e., about 5 lifetimes of the excited anion. Data taken from Refs 35, 36.

within the electric field of the central anion. As long as the proton is within the Coulomb cage ($R_0 < r < R_D$) the diffusion is biased by the electric force. This model suffices for quantitative analysis of experimental observation and determination of the parameters defined in the scheme.

The scenario described above was transformed into differential equations [35] which reconstruct the dissociation of proton from photoexcited molecules of pyranin. By this procedure one can vary selectively the magnitude of each parameter and examine how it affects the dynamics. The outcome of these computations is given in Fig. 5, where in each fame only one variable is adjusted. The heavy line is the one best simulating the experimentally measured dynamics.

Fig. 5A demonstrates the effect of the electric field (given as $R_D$) on the undissociated fraction of pyranin. Whatever is the size of $R_D$ (increasing from 10 Å to 100 Å), the initial rate of dissociation is identical, but the dynamics acquire a 'tail' which increases in size. For very large $R_D$ (100 Å), frequent recaptures will make 50% of the population appear as undissociated. An external observer, unaware of geminate recombination, will mistakenly assume that the p$K$ of the compound is much higher than its actual value.

In Fig. 5B, the size of the contact radius is the variable. A large contact radius of 12 Å or more (not shown) places the proton far enough away to make its escape from the cage relatively easy. As the contact radius shrinks, the electric field increases in intensity. Under such intensive attraction, the probability of escape declines sharply, leaving a major fraction of the population in the undissociated state.

The diffusion of the proton within the cage is investigated in Fig. 5C. A small diffusion coefficient will slow the random walk of the proton, amplifying the effect of the electrostatic bias on the proton's trajectory. The proton will remain for a longer period close to $r = R_0$ where the electric field is maximal and more recombinations will ensue.

The effect of the 'chemical' terms is demonstrated in Fig. 5D and E. The rate of covalent bond breaking and replacing it by hydrative stabilization ($k_d$) controls the initial rate of dissociation. As a matter of fact, it is the only parameter which controls this step. Thus, time-resolved measurements can determine accurately the rate of this reaction. The importance of this 'obvious' conclusion will be discussed below. The effect of covalent bond reformation ($k_r$) is shown in Fig. 5E.

Looking at the five frames demonstrates that each parameter affects the dynamics in a different way. Yet there is only one combination which can reproduce accurately the observed experimental curve (Fig. 5F) and with such accuracy that the predicted curve practically eclipses the experimental points [35].

The formalism of Agmon, Huppert and Pines [30,35,36] is a stepping stone for understanding much more complex systems. It provides for a unique identification of the initial phase of the measured dynamics with a single, undirectional chemical event: the forma-

tion of the ion pair. Whatever follows in time is the mixture of all reactions: dissociation geminate recombination and separation.

In a system where ions are separated with no recombination, the time constant of pair formation ($\tau_{off}$) can be calculated from the relative quantum yield of $\phi OH^*$ emission ($\Phi_{\phi OH^*} = I_{\phi OH^*}/I_{\phi O^{*-}}$) and the fluorescence lifetime of $\phi OH^*$ ($\tau_f$) using the expression of Weller [37]:

$$\Phi_{\phi OH^*} = \frac{\tau_{off}}{\tau_{off} + \tau_f} \tag{5}$$

As $\Phi_{\phi OH^*}$ and $\tau_f$ are independently measured, $\tau_{off}$ can be calculated. In the case where the ion pair recombination is minor there is a good agreement between $\tau_{off}$ and $k_d^{-1}$ ($\tau_d$), which is determined directly by fast kinetic measurements. When geminate recombination is aprpeciable and the decay of $\phi OH^*$ gains its long tail, the value calculated according to Eqn. 5 will become an average of the initial charge separation and the ensuing recombination process. In this case we shall refer to it as the relative quantum yield value,

$$\tau_{RQY} = (\tau_{off} + \tau_f) \cdot \Phi_{\phi OH^*}.$$

There is a clear correlation between the time constant of ion pair formation $\tau_d$ and the average value $\tau_{RQY}$. Whenever $\phi OH^*$ is formed, a period, $\tau_d$, will elapse (on the average) before it dissociates. Thus, the average dissociation time, $\tau_{RQY}$, is equal to the intrinsic dissociation time ($\tau_d$) plus the product of $\tau_d$ times the average number of geminate recombinations. As both $\tau_{RQY}$ and $\tau_d$ are experimentally measured, we can calculate the average number of recombinations as $(\tau_{RQY}/\tau_d) - 1$. This expression is inconvenient for comparison between different compounds. The one with the longer lifetime of the excited anion ($\tau_{\phi O^{*-}}$) will experience more encounters before it decays to the ground state. For this reason it is better to calculate the average time lapse between the repeated recombinations as given below:

$$\tau_{gem.recom.} = \frac{\tau_{\phi O^{*-}}}{(\tau_{RQY}/\tau_d) - 1} \tag{6}$$

The application of Eqn. 6 for analysis of complex systems will be demonstrated in subsection III-D (see below, Fig. 11).

*II-C.3. Proton transfer in buffered systems*

Until now our interest has been limited to ideal systems where, besides water, there is no other species reacting with the ionized pair. Physiological systems are well buffered both by small solutes and the side-chain of macromolecular structures; their involvement in observed proton transfer must be clarified.

In equilibrium systems buffers are commonly regarded as silent assistants that maintain a constant pH but do not alter the observation. In dynamic systems the buffer assumes a central role affecting both rates and mechanism. It affects the events by functioning as carrier which clears the proton from site of the reaction, by serving as a primary proton acceptor or providing an alternative path which functions in parallel with the proton dissociation-diffusion route.

*II-C.3a. The role of buffer in clearance of protons.* A protogenic catalytic reaction produces a proton in the active site and, unless it is effectively removed, its accumulation in the vicinity may inhibit the progress of the reaction. Addition of buffer to the reaction medium will relieve the restraints, substituting the diffusional clearance of protons by chemical trapping.

This concept was proposed by Engasser and Horvath [38] who quantitate it by the ratio of proton production rate to its clearance rate from the site. Their calculation demonstrated that, as long as the ratio is low (less than $10^{-5}$), the system behaves normally; the pH in the active site will be that of the bulk, while the velocity vs. pH curve corresponds with the properties of the active site. At a production/clearance ratio larger than $10^{-4}$, the pH in the active site differs from the bulk, and accumulation of protons will suppress (or reverse) the reaction. This situation can be readily detected as a change of catalytic velocity and pH optimum upon addition of buffer. Such restrictions are expected when the enzyme is immobilized on a membrane [39], when rate of catalysis is very high (carbonic anhydrase [40]) or due to structural constraints imposed by the microscopic folding of mitochondrial cristea [41].

*II-C.3b. Effect of buffer on proton concentration gradient.* The average lifetime of a free proton in solution is given by $\tau = 1/(k_a \cdot A^-)$ where $k_a$ is the rate of association with the acceptor, $A^-$. In pure water at pH 7, where $OH^-$ is the only acceptor, $t = 100$ $\mu$s. At the same pH, in the presence of 1 mM of buffer ($k_a$ for most acceptors is $(1\text{–}3) \cdot 10^{10}$ $M^{-1} \cdot s^{-1}$, see Table I) the mean lifetime is $\tau \approx 30$ ns. Thus the kinetic effect of buffering a solution is to shrink the delay between proton dissociation-recombination events to a nanosecond time frame. The short duration of free proton reduces the average distance it can diffuse within its lifetime, and the dimension of nonhomogeneous proton dispersion. A protonogenic site modulates the proton concentration in its most immediate vicinity. The dimension of this local effect is comparable with $l = \sqrt{6D\tau}$, where $\tau$ is the lifetime of the free proton. Thus, even a low buffer concentration (10 mM) suffices to reduce $d$ to about 15 nm. Beyond this range the incremental proton concentration is replaced by an incremental $BH/B^-$ ratio. As a result, the free proton gradient in buffered solutions will be steeper than in an unbuffered one. This can have a direct effect on velocity of reactions where $H^+$ (not BH) is a reactant, like proton flux through a neutral proton channel [42]. The flux is

driven by the difference in proton concentration between the two sides of a membrane and the velocity is determined both by the pore permeability and the convergence permeability (the rate at which the ion diffuses from the bulk to the orifice of the pore). In buffered solution the convergence permeability will increase due to the shorter distance $H^+$ must diffuse before it enters the mouth of the channel.

*II-C.3c. The apparent diffusion coefficient in buffered solution.* The buffering of biological system consists of two types of buffer: mobile solutes and protonable groups of macromolecular structures like proteins or membranes. Both contribute to the buffering capacity, yet their effect on the propagation of proton in the reaction matrix is very different.

Fixed buffer molecules will bind the proton for a long period of time (see Fig. 4), thus reducing the apparent diffusion coefficient by the fraction of the protonated buffer [43]. Mobile buffers will also reduce the free proton concentration, but due to their diffusivity ($\approx 10\%$ of free proton) they will have a milder effect on the effective diffusion of coefficient. In the presence of both mobile (M) and fixed (F) buffer, the effective diffusion coefficient will depend on the total buffer capacity $\beta_{tot}$, the relative contribution of M and F to $\beta_{tot}$ and the diffusion coefficient of MH ($D_{MH}$).

The quantitative solution for such complex system was derived by Junge and McLaughlin [44] as a general form of Fick's law

$$\frac{\partial([H^+]+\Sigma_i[HB_i])}{\partial t} = \frac{D_H \partial^2[H^+]}{\partial x^2} + \frac{\Sigma_i D_i \partial^2[HB_i]}{\partial x^2}$$

which states that within an infinitesimal volume the rate of accumulation of acidic forms (free $H^+$, protonated mobile buffer ($HB_{Mi}$) and protonated fixed buffer ($HB_{Fi}$) is equal to the divergence of flux of mobile acidic forms ($H^+$ and $HB_{Mi}$) into this space.

The solution to this equation leads to the expression for apparent diffusion coefficient:

$$D_{app} = \frac{D_H + \dfrac{D_{HM}[M^{tot}]}{K_M}}{1 + \dfrac{[M^{tot}]}{K_M} + \dfrac{[F^{tot}]}{K_F}}$$

As seen from this expression, addition of any buffer (fixed or mobile) to the system will hinder the diffusion of the proton. Yet not all buffers will have the same effect. Very acidic compounds, $pK \ll pH$, will have a negligible capacity to bind the proton, while basic ones will hardly dissociate. Thus a better expression will be one which scales the buffers according to their contribution to the total buffer capacity:

$$D_{app} \approx D_H\left[\frac{2.3[H^+]}{\beta^{tot}}\right] + D_{OH}\left[\frac{2.3[OH^-]}{\beta^{tot}}\right] + \frac{\Sigma_i D_i \beta_i}{\beta^{tot}} \qquad (7)$$

This expression combines for the diffusion of $H^+$, $OH^-$ (thus covering the $pH > 7$ range) and the contribution of all buffers present weighed by their buffer capacity ($\beta_i$) at the given pH. Immobile buffers like proteins or phospholipids will contribute only to the total buffer capacity, appearing in the denominator. A mobile buffer will contribute both to the nominator and denominator and will not slow the diffusion as much as immobile one.

The validity of this expression was demonstrated experimentally [45]. The partition space of stacked thylakoids is heavily buffered by the proteins on the membrane surface which, due to their almost zero diffusibility, slows the $OH^-$ diffusion by 5 orders of magnitude with respect to that in bulk. Addition of 1 mM phosphate provides sufficient mobile carrier to increase the flux of acidity in the matrix.

The apparently slow propagation of protons on a membrane's surface originates at a molecular level from a combination of two factors: a long dwell time of the proton on the fixed buffer moiety (in accord with Fig. 4) and a high probability that a proton released by one fixed buffer moiety will be recaptured by a nearby group. The precise quentitation of the recepture calls for another type of information, that emerging from time-resolved kinetics.

*II-C.4. Collisional proton transfer: an alternative proton route*

The role of buffer, as discussed above, relied on the convenience of physical simplifications to an extent which made the mathematical expressions suitable for analytical solution. This vantage point is gradually lost upon increasing the complexity of the system, especially when the same product may be formed by more than one route.

A comprehensive analysis of proton transfer in multicomponent systems, which is a common situation in any biochemical system, must rely on a two-step strategy. At first the observation is treated by chemical kinetic methods to determine the rate constants of the individual reaction (using relaxation kinetic expressions [46] or numerical methods [47,48]). In the second phase, the rate constants are subjected to physical interpretations to derive characteristic parameters like diffusion coefficients, local viscosities or electrostatic interactions [29].

*II-C.4a. Measurements of reaction rates.* Determination of the rate constants of fast protonation reactions must employ a time-resolved fast-kinetic methodology. When the reactants are fairly dilute ($10^{-6}$–$10^{-7}$ M), microsecond resolution is required. The most convenient method we know for this purpose is the Laser-Induced Proton Pulse (Refs. 47, 48 but see also Refs. 49, 50). This is a general delta perturbation method, unrestricted by the ionic strength of the solution (which is

a severe limitation for electric field jump). The perturbation can be applied repetitively, which makes it convenient for averaging measurements without losing the time resolution.

The key reaction is a photoexcitation of aromatic alcohols ($\phi$OH) or nitrogen heterocyclic ($\phi$N) compounds to their first electronic singlet state. In the excited state, the p$K$ of the compound is much smaller than in the ground state ($pK^* \ll pK$ as for $\phi$OH compounds) or much higher ($pK^* > pK$, as for $\phi$N compounds). Within the few nanoseconds lifetime of the excited state there is a fast interaction with the solvent leading to proton dissociation ($\phi OH^* \rightarrow \phi O^{*-} + H^+$) or proton abstraction ($\phi N^* + H_2O \rightarrow QNH^{*+} + OH^-$) with a yield of 10–50 $\mu$M of either $H^+$ or $OH^-$ generated within these few nanoseconds. When the excited state relaxes to the ground state, the system is locked in a state of disequilibrium; $H^+$ (or $OH^-$) concentrations differ markedly from that compatible with the concentrations of all other compounds present in the perturbed space. The discharged protons react with all protonable groups, upsetting their state of equilibrium. The perturbation finally relaxes when the protonation state of the ground state emitter returns to the prepulse state. The whole transient cycle is monitored either by spectrophotometric [47,48] or potentiometric [51–53] methods.

The measured signal is subjected to rigorous analysis which reproduces the experimental observation by numerical integration of coupled differential equations pertinent to the measured system. The convenience of writing differential equations and the availability of integration programs allows us to investigate systems where four (or even more) reactants interact simultaneously with $H^+$ and with each other. The numerical solution of complex systems (like proteins) or membrane protonation dynamics led to consistently accurate rate constants with less than $\pm 20\%$ error (see Table I).

The manifold role of collisional proton transfer in a multicomponent system is demonstrated by the following pOH jump experiment (see Fig. 6). Photoexcitation of 6-methoxyquinoline shifts its p$K$ from 5.1 to 11.9. Within the 4 ns of its lifetime it abstracts a proton from the water and, upon relaxation, a $\phi NH^+$ and $OH^-$ pair is formed [26]. A pH indicator (Bromothymol blue, p$K$ 7.1) present in the solution will either be deprotonated (by $OH^-$) or protonated (by collision with $\phi NH^+$), depending on the initial conditions. At $pH < pK_{BTB}$, most of the indicator is initially protonated, so the dominant reaction is deprotonation of BTB-H by $OH^-$ (trace A in Fig. 6). The scenario is totally transformed in the presence of 20 mM Tricine buffer ($pK = 8.0$). At the same pH, the highly abundant BH reacts preferentially with $OH^-$, while collisional protonation by $\phi NH^+$ increases BTB-H concentration (trace B in Fig. 6A). At higher pH the outcome of the same perturbation is different. The abundant BTB state is protonated by collision with $\phi NH^+$, leading to a large protonation transient lasting almost 300 $\mu$s. The effect of buffer at this pH is more conventional. The buffer competes with $In^-$ for the $\phi NH^+$, lowering the amplitude and accelerating the relaxation of the protonated indicator (curves A to C in Fig. 6B).

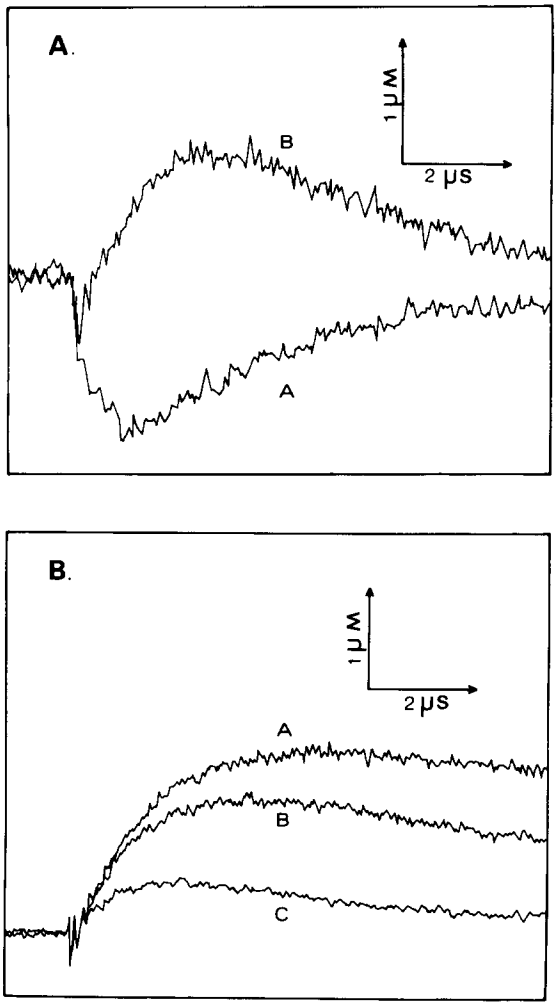


Fig. 6. Transient absorbance associated with fast pH perturbation of Bromothymol blue solution by pulse excitation of 6-methoxyquinoline. Upward deflection corresponds with acidification of the indicator. (A) Trace A depicts a rapid deprotonation of the indicator by $OH^-$ generated by the pulse. Trace B was measured under same conditions except that 20 mM Tricine buffer was added. Note that after brief deprotonation, lasting a few microseconds, there is a major phase of protonation of the indicator. The experiment was carried out in presence of 2 mM methoxyquinoline as photoactivated base, 50 $\mu$M Bromothymol blue at pH 6.58. (B) The same experiment as above carried out at pH 8.0. Trace A, no buffer; traces B and C, in presence of 1 mM and 10 mM Tricine. (Data taken from R. Yam's dissertation, Ref. 84.)

This simple system sufficies to demonstrate the manifold effects of collisional proton transfer on the observed dynamics. It provides a network of parallel, competing reactions which can be resolved only upon integration.

The rate constants of collisional proton transfer reactions, in the thermodynamically favoured direction, fall in the range of $10^8$–$10^9$ $M^{-1} \cdot s^{-1}$ (see Table I in Ref. 47). Because of this fast reaction, even a few millimolar concentration of buffer suffices to support a submicrosecond proton exchange reaction, a rate much faster than proton dissociation events. In bioenergetic systems, transfer of acidity between sites will be carried mostly by proton exchange between small solutes.

*II-C.4b. Reactions on the interface.* The distance between protonatable sites on protein surface, or a phospholipid membrane, can be comparable to the Coulomb cage radius of the individual moieties. In these cases the almost overlapping cages merge into a continuum [54], so that recapture of a released proton becomes highly probable as in a geminate recombination.

The rate constant of proton exchange between sites on a surface was measured by the same mode described in previous sections. In most cases the rate constants are about $10^{10}$ $M^{-1} \cdot s^{-1}$. It must be explicitly stated that the rate constant is given in $M^{-1} \cdot s^{-1}$ units, which formally are reserved for second-order reactions. The mechanism of recapture is not a simple second-order reaction, thus the rate of these reactions can be used only for comparison among them, not to be compared with rate constants where one of the reactants is diffusing in solution.

*II-C.4c. Bulk surface proton transfer.* The exchange of protons between surface and bulk is a sum of all mechanisms operating in the system under study, and the contribution of collisional proton transfer to the total flux is appreciable [55]. A demonstrative experiment, given in Fig. 7, is the protonation of a micellar bound indicator, Bromocresol green, by proton generated in the bulk [56]. The dynamics (trace A) consist of diffusion-controlled protonation of the indicator followed by a slow relaxation. Both the amplitude and the rate of relaxation are modulated when phospholipids are incorporated into the micelle. Addition of phosphatidylcholine, with $pK = 2.25$, increases the amplitude by almost 50%, while higher-$pK$ phospholipids (phosphatidylserine, $pK = 4.6$ (trace C), and phosphatidic acid, $pK_2 = 8.0$ (trace D)) lower the amplitude.

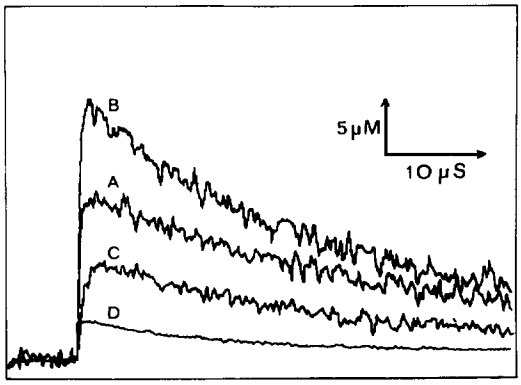


Fig. 7. The effect of phospholipid headgroup on the protonation dynamics of an indicator adsorbed on a surface of neutral micelle. The indicator, Bromocresol green, was adsorbed on Brij-58 micelles at ratio of one per micelle. The pulse protonation, measured at pH 7.3, was initiated by photoexcitation of a water-soluble proton emitter 2-naphthol 3,6-disulphonate (2 mM). The reaction was followed spectrophotometrically. (A) Control. No phospholipids added. (B) Phosphatidylcholine added to amount of 6 molecules per micelle. (C) Phosphatidylserine added to 6 molecules/micelle. (D) Phosphatidic acid added to 6 molecules/micelle. For more details see Nachliel and Gutman [26].

The rate constant of proton exchange among the surface groups corresponding to traces B, C and D are the same ($10^{10}$, see Table I, Ref. 56), indicating that, in all cases, the proton recepture is of comparable probability. The major difference between the three phospholipids is the mean time for the temporary proton binding by each compound. Because of its low $pK$, the phosphatidylcholine retains a proton for only a few nanoseconds between successive dissociation (see Fig. 4). The short delay (on the site) and high recapture probability of the surface groups allow the proton to make many random steps within a given time frame, which increases the efficiency of the search for the surface-bound indicator [57,58]. This is observed as a larger probability of protonation (compare trace A to B).

A surface moiety with higher $pK$ (phosphatidylserine) retains the proton for about 2 μs between successive dissociations. Within the average lifetime of the proton on the surface (for more rigorous formalism see Berg and Purcell [58], especially Eqns. 15–19), less excursion steps will be taken and the protonation of the indicator is diminished by 50%. Similar effects have been measured for protonation of specific sites on proteins [59].

## III. Proton diffusion within geometrically constrained space

### *III-A. The geometry of the reaction space*

Bioenergetically important protogenic reactions proceed at the active sites of membranal proteins. Structurally, these sites are extremely unisothropic. Part of the site is exposed to the solvent while the rest is bounded by proton impermeable structure made of protein and/or membrane. This structural element affects both dynamic and equilibrium of protonation by two linked elements:

(A) A water molecule in contact with the boundary structure exhibits a preferred orientation with respect to the surface. Such a persistent orientation will change the diffusion coefficient of $H^+$.

(B) A reflecting (or non-permeant) structure will bias the random diffusion process, directing the proton toward the bulk.

The contribution of both elements to the observed dynamics of proton transfer varies with the observation time. As long as the proton is diffusing in a homogeneous matrix, the reaction evolves as spherically symmetric. If an inhomogeneity such as boundaries are present, the probability of proton capture deviates from bulk conditions. For a given length ($l$) of homogeneous matrix, any oservation lasting more than $\tau = l^2/D$ will already bear the mark of the inhomogeneous reaction space, affecting the rates and equilibrium constants. The length of a homogeneous, unobstructed proton path in bioenergetic structures is short, varying from about 10 Å (as an active site or proton channel) to a few hundred ångströms (the spacing between membranes in swollen mitochondria or chloroplast). Approximating a bulk value for $D_{H^+}$, we find that only observations lasting few nanoseconds are free of geometric modulations. In other words, all (or most) of the kinetic and equilibrium constants of bioenergetic proton transfer incorporate the contribution of the microscopic heterogeneity of organelles and enzymes.

The concept that architectural elements modulate proton transfer dynamics is common in bioenergetics. It is usually invoked to accommodate experimental pecularities within the framework of the chemiosmotic theory. De Kouchkovsky et al. [60] envisioned a network of intramembranal proton-conducting tunnels, connecting sink and sources in a 'bulk secluded' passage. It was even contemplated how the conductivity of the proton guide will vary upon swelling of the organelles. Similar concepts were proposed also by Dilley and Nagle [61], Theg et al. [62] and Pick [63]. A more exotic concept, the electrodic view, envisions proton streaming on the membrane/water interface, insulated from the bulk by the Helmholtz layer * [64]. There is a common feature for all these models: the experimental evidence on which they are based is quasi-equilibrium or steady-state kinetics. These observations are per definition 'blind' to any event faster than the overall rate-limiting step. As all these studies relied on enzymic reaction for driving a proton flux, their time reliability is, at most, in the millisecond range. Bulk surface proton exchange is sufficiently rapid to reach equilibrium in the submicrosecond time-scale, i.e., $10^3$–$10^6$ times faster than the enzymic reaction [13,18,29,47,48,50,51,55,56,59]. Consequently, the experimental evidence referred to in Ref. 60–64 is unsuitable for drawing conclusions about the dynamics of proton on a surface.

It is not our intention to scrutinize or evaluate the acceptability of these scenarios. We shall rather investigate, by proper time resolution, what will be the effect of such structural elements on well-known proton transfer reactions as they proceed in geometrically defined, experimentally controllable reaction space. The conclusion derived from these studies, as detailed below, shouls be applied for evaluating the feasibility and acceptability of bioenergetic models relying on 'localized proton transfer'.

### *III-B. Diffusion of proton in bound water*

Any boundary within liquid water will affect the organization of the water molecules adjacent to the discontinuity. Because of the asymmetric structure of $H_2O$, a preferred orientation is imposed which builds an approx. 100 mV electric field within the first ångström from the wall, i.e., within the width of the adjoining water molecule [65]. This ordering of solvent has been experimentally observed. The X-ray structure of protein reveals clusters of water molecules not only between hydrophilic regions but especially around hydrophobic regions. On the surface of these supposedly 'noninteracting' structures, pentagonal water clusters containing up to 16 ordered water molecules were observed [66].

The nature of the water molecules at an interface was studied by time-resolved fluorescence of tryptophan residues of proteins adsorbed to the surface of reversed micelles [67], where the micelle's water content is an experimentally controllable parameter. When the peptide was transferred from bulk water to the aqueous space of reversed micelle there was a severe slowing of the peptide internal dynamics, expressed as strong limitation of the rotation of the tryptophan residues. Residues located closer to the water/surfactant interface were more affected, demonstrating a gradient in the properties of the solvent enclosed within the reversed micelle.

The gradient of water at an interface can be measured by the technique of Parsegian, Rand and their colleagues (for review see Ref. 68) and Israelashvili [69] and his co-workers, who measured the distance between phospholipid surfaces under external pressure. Such studies indicate an exponential variation of the activity of water through the first 3–5 water layers of the hydration layer. As we discussed before (II-B.2), the diffusion coefficient of proton is very much influenced by the frequency of randomization in the percolating network of hydrogen-bonded water molecules. Thus, in parallel with the water activity, the mobility of the proton will vary with its distance to the surface. For this very reason membranes are models too complex for

* The Helmholtz layer is a kinetic barrier, formed on a surface of electrode during electrochemical reaction. The origin of the barrier is the higher conductivity of the electrode with respect to the electrolyte solution. Thus, the rate of product formation on the electrode surface is faster than its dispersion into the unstirred layer. Under such conditions a barrier is formed at the interfaces and the rate-limiting step is the flux of product across it. The catalytic turnover of protogenic reactions ( $\approx 1$ ms) is much slower than the dissipation of proton to the bulk. Thus the kinetic barrier is non-existent.

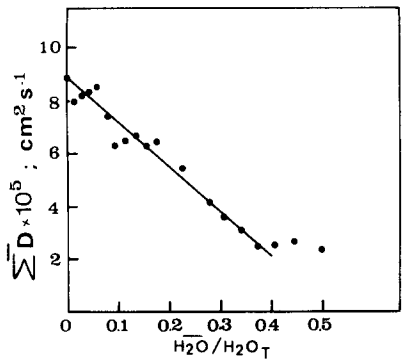


Fig. 8. The dependence of the diffusion coefficient of proton on the fraction of bound water as measured in sucrose solutions. The value denoted by the ordinate is the sum of the diffusion coefficient of $H^+$ and the pyranin anion. This value is actually identical with that of the proton ($\overline{\Sigma}D = D_{H+}$). The diffusion coefficient is already corrected for the obstruction of the path by the proton-impermeable sucrose molecules [72]. The fraction of bound water, given by the abscissa, was calculated from data given in Ref. 70 (Ophir and Gutman, unpublished results).

investigating how ordering affects proton diffusion; the results will reflect both gradient of $a_{H_2O}$ and the contributions of the surface per se (see below).

The suitable systems for measuring proton diffusion in bound water are concentrated solutions of sucrose. Each sucrose molecule binds very tightly 7.7 water molecules [70], but as they are oriented in all directions, the dielectric constant of the solution remains high. The rest of the water molecules in the solution are essentially free and their activity coefficient is very close to unity [70]. In concentrated sucrose solution, the fraction of bound water can be as much as 50% of total water present.

The diffusion of proton in concentrated solutions of sucrose was measured by photodissociation of a proton from pyranin and measuring the recombination of the proton with the resulting ground-state anion. The measured rates were analysed to determine the second-order rate constant of the reaction and subjected to analysis according to the Debye-Smoluchowski equation (Eqn. 4). The diffusion coefficient ($D_{H+}$) was calculated with correction for the dielectric constant, electrostatic screening and the excluded volume of sucrose molecules through which protons cannot diffuse [71]. It was observed that $D_{H+}$ was independent of the viscosity of the solution [72] but decreased as the fraction of bound water was increased. This dependence is shown in Fig. 8. The negative slope of the line and levelling at about 20% of the value of $D_{H+}$ in bulk water imply that bound water is a poor matrix for proton diffusion.

Based on this observation we project that the proton mobility will vary steeply through the hydration layer. It will be minimum at contact with the surface, reaching the bulk value at distance of 3–5 water molecules. In such an inhomogeneous matrix the gradient of mobility will bend the diffusion trajectories, directing the flux of proton towards the bulk.

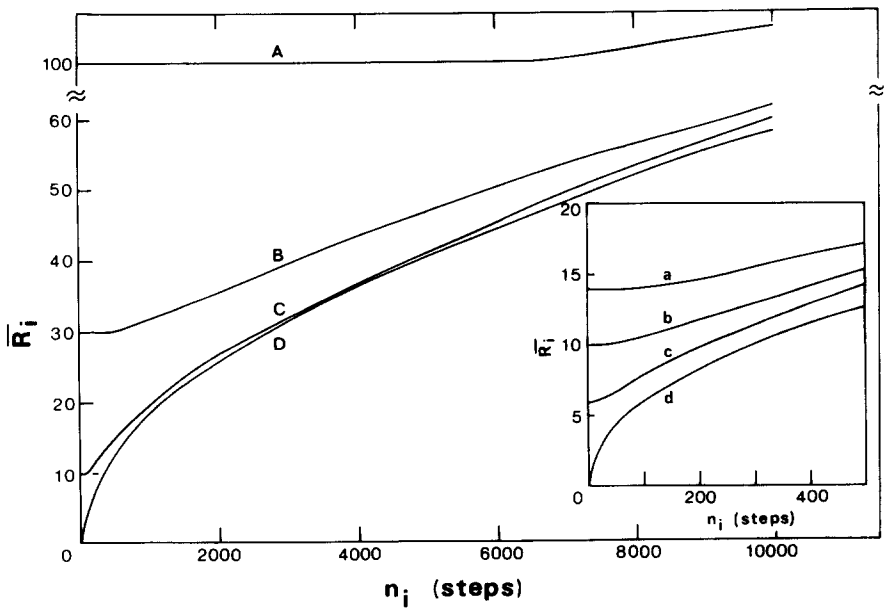


Fig. 9. A computer simulated scenario of a diffusion of particle released at a given distance from a reflective non-interacting surface. The average position ($\overline{R}_i$) is calculated after each diffusion step ($n_i$) for a large number of particles all released at the same point. Curve A depicts the behaviour of particle generated at a distance of 100 diffusion steps from the surface. During the first 6000 steps or so, the particles can move in all directions so that the average distance is invariable. After that period some of the particles have reached the vicinity of the reflecting surface and their diffusion is not random any more. Some of the diffusion steps are not permitted. As a result the average distance of the whole population is affected and $\overline{R}_i$ gradually increases. As the initial position gets closer to the surface (curves B to D) the drifting begins after a shorter period. The inset expands the first 500 steps for initial distance of 13, 6, 3 and 0 for curves a to d, respectively. For details see Ref. 73.

*III-C. The effect on a non permeable surface of the mean position of a diffusing particle*

To evaluate how a non-permeable surface affects the trajectory of a diffusing particle, Gutman et al. [73] conducted a set of computer experiments simulating a particle diffusing in a continuum matrix. The algorithm employed was a random selection of direction in a three-dimensional space and taking a unit length step in that direction. The only restriction introduced was that whenever the step would carry the particle across a defined planar surface, the motion was forbidden and reselection of direction took place.

The calculations were carried out for a population of 1000 non-interacting particles, all released from the same point at a given distance ($R_0$) from the reflecting wall. The mean position of the particles, as averaged for the whole population, was drawn as a function of the number of diffusion steps (Fig. 9).

A particle released far from the surface may select any direction for its stride, so that the average position of the population will not vary with time (curve A). After many random steps, some of the particles approach the surface. This fraction of the population is subjected to steric hindrance on its direction selection. The rest of the trajectories continue to evolve in an unbiased way so that the mean position of the population slowly drifts away from the surface.

As the initial release distance decreases, the time point at which some of the trajectories contact the non-permeable plane is shortened and a larger fraction of the population is affected. Thus, as $R_0$ decreases from 100 to zero, the rate of the drift increases (curves A to D).

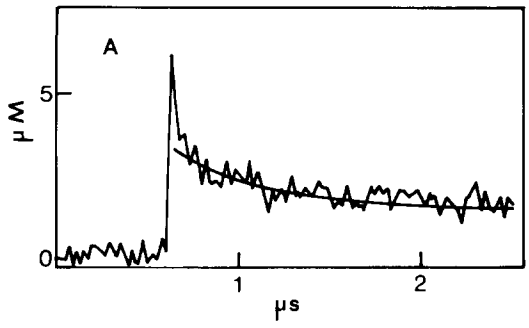


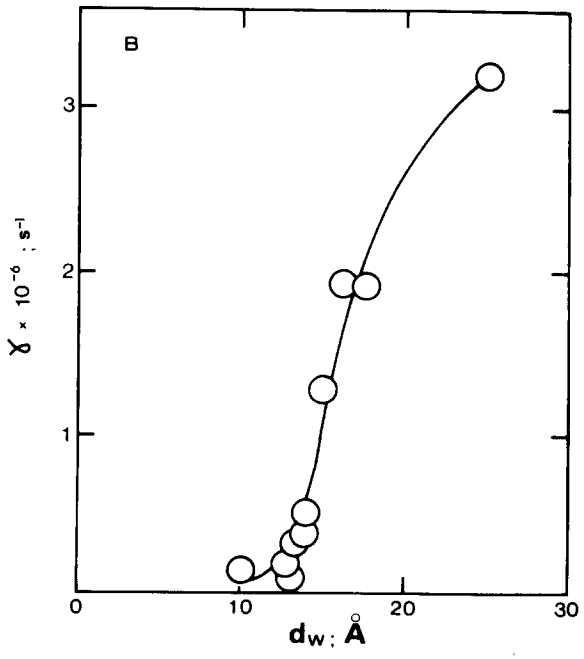


Fig. 10. (A) Time-resolved dynamics of the reprotonation of pyranin anion as taking place within the aqueous lamella of multilamellar vesicle made of egg phosphatidylcholine. The dye was photodissociated by a short laser pulse and the absorbance of the resulting ground-state anion was followed with time with a 10 ns resolution. The continuous smooth curve is a reconstructed dynamics generated by the rate constants given in Table II. For details see Gutman et al. [29]. (B) Dependence of the observed rate of reprotonation ($\gamma$) on the width of the hydration layer. The experiment, as in (A), was carried out with the same vesicle preparation under verying osmotic pressures. The width of the hydration layer, $d_w$, was calculated from the data of Parsegian et al. [78]. (C) Dependence of the observed rate of reprotonation on the two-dimensional concentration of pyranin anion in the hydration layer. The rate constant ($\gamma$) was calculated from the experiments carried out as in (A). The concentration of the anion was calculated from the amplitude of the transient and the dye/lipid ratio of the preparation. The magnitude of the amplitude was varied by modulating the energy of the excitation laser pulse. (A) Measurements were carried out in the absence of sucrose. (B) Measurements were carried out in the presence of 0.57 molal sucrose ($1.5 \cdot 10^7$ dyn/cm$^2$).

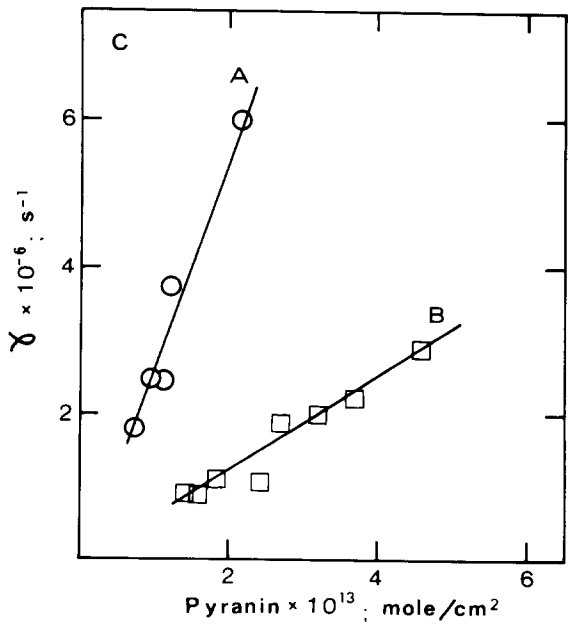

These calculations demonstrate that, in the absence of long-range forces, a non-permeable surface affects the diffusion of particles, even at a distance. In the same sense, protons generated by protogenic site on a membrane (a population characterized by $R_0 = 0$, curve D) will by random walk drift away to the bulk.

*III-D. Diffusion of proton in thin water layers*

The diffusion of proton within the hydration layer is preferably measured in an experimental system where diffusion is limited to aqueous layers insulated from the bulk water. For an unambiguous interpretation of the results, the time-scale of the observation should be short, comparable to the rate of the reaction. This restriction ensures that slow redundant events will not affect the observation.

These requirements are not met by the experimental model of Prats, Toccane and Teissie [74,75]. In their experiments acid solution was injected by syringe to a well-stirred compartment in a trough, and the protons were detected at an approx. 5 cm distance by acidification of a fluorescent probe incorporated in a monomolecular phospholipid layer spread over the water/air interface. These observations were analyzed by a random walk computer stimulation program [76] over a small square grid ($6 \times 30$). According to this model, the apparent diffusion coefficient of proton at the interface is about 20-times larger than in the bulk. The observation was experimentally criticized [77] on the basis that stirring of the acidifed compartment was essential for the observation. It was also pointed out that an apparent diffusion coefficient on the surface which is 20-times larger than the bulk value necessitates an actual microscopic diffusion coefficient which is $10^6$ larger than in bulk [77]. Only such an unacceptably high value will compensate for the tendency of protons at the surface to be diluted in the bulk.

To avoid the controversy of massive bulk volume equilibrated with the ultrathin hydration layer, Gutman et al. [29] analyzed proton diffusion in the aqueous lamella sandwiched between phospholipid membranes in multilamellar vesicles. The vesicles were made by swelling of dried phospholipid in dilute (2 mM) aqueous solution of pyranin. By this procedure the dye is entrapped almost exclusively in the few outermost aqueous layers [29]. The proton-emitting dye is confined to a topographically defined environment; the composition of the phospholipid membrane is known, while the width of the aqueous lamella is regulated by external osmotic pressure [68]. Within these structures the diffusion of the proton can be measured with a submicrosecond time resolution.

The observed kinetics are shown in Fig. 10A. At the indicated point, a 10 ns laser pulse dissociated a proton from the trapped pyranin, and the reprotonation of the ground state anion was monitored by time-resolved absorbance measurement. In unpressed egg PC multilamellar vesicles ($d_w = 28.5$ Å [78]), proton recombination is characterized by a relaxation constant of about $3 \cdot 10^6$ $s^{-1}$ (see Fig. 10B). In the presence of osmotic pressure, as $d_w$ decreases, the rate of recombination is slowed to almost 5% of the relaxed system. The conclusion from these observations is that the diffusion of proton in the ordered water of the interface [65–67] is slower than in bulk water. Quantitative evaluation of the diffusion coefficient was obtained by two analytical procedures: two-dimensional and spheric symmetric approximations.

The *two-dimensional approximation* identifies the diffusion space as a plane at the centre of the hydration layer, which has the highest value of $a_{H_2O}$. In a two-dimensional space the relation between the apparent rate constant ($\gamma$), reactant concentrations (mol/cm$^2$) and diffusion coefficient ($D_{(2)}$) is given by the equation derived by Hardt [78].

$$D^{H}_{(2)} = \frac{\gamma}{2\pi N[\phi O^{-}_{(2)}]} \ln \frac{1}{R_0 \sqrt{\pi N[\phi O^{-}_{(2)}]}} \qquad (8)$$

According to Eqn. 8 and under the experimental conditions defined in Fig. 10A, there should be a linear dependence of the apparent rate constant on the amplitude ($\Delta\phi O^-$) with a slope proportional to $D^{H^+}_{(2)}$. Analysis of the results according to Eqn. 8 is given in Fig. 10C. The two sets of experiments measured at $d_w = 28.5$ Å and 15 Å yielded diffusion coefficients of $D^{H^+}_{(2)} = (2.5 \pm 0.5) \cdot 10^{-5}$ cm$^2$/s and $0.65 \cdot 10^{-5}$ cm$^2$/s, respectively.

The *spheric symmetric* approximation treats the reaction as if proceeding in a homogeneous solution with a concentration of phospho moieties corresponding to the reciprocal aqueous volume available for each phospho headgroup. In the absence of any external pressure each phospholipid headgroup shares about 930 Å$^3$ of the aqueous layer. This volume is 1.8-times smaller than that available for a molecule in 1 molar solution, a reminder of the very special conditions prevailing in bioenergetic organelles, where thin water layers are bounded by highly buffered surfaces [44].

To determine the individual second-order rate constants, Gutman and his colleagues [29] considered in their analysis both proton dissociation diffusion reactions as well as collisional proton exchange between all reactants present in the water layers. Numerical integration of differential rate equations generated the continuous curve appearing in Fig. 10A.

The second-order rate constants were analysed according to the Debye-Schmulochowski equation to derive both $D_{H+}$ and the viscosity of the water in the hydration layer (see Table II).

The values clearly indicate that the diffusion coefficient in the hydration layer is smaller than in bulk water

TABLE II

*Kinetic constants of proton transfer reactions and physical properties measured in hydration layers in phosphatidylcholine multilamellar vesicles*

| | | |
|---|---|---|
| Sucrose (molal) | 0 | 0.57 |
| Osmotic pressure (dyn/cm$^2$) | $5\cdot10^5$ [a] | $1.5\cdot10^7$ |
| Width of hydration layer [b] (Å) | 25 | 15 |
| Rate constant of reprotonation ($M^{-1}\cdot s^{-1}$) | $(5\pm1)\cdot10^{10}$ | $(2\pm1)\cdot10^{10}$ |
| Diffusion coefficient of proton ($cm^2\cdot s^{-1}$) | $10\cdot10^{-5}$ [c]<br>$2\cdot10^{-5}$ [d] | $4.4\cdot10^{-5}$ [c]<br>$1\cdot10^{-5}$ [d] |
| Rate constant of $\phi O^-$ reaction with PC-H ($M^{-1}\cdot s^{-1}$) | $1\pm0.5\cdot10^9$ | $4\pm0.5\cdot10^8$ |
| Diffusion coefficient of $\phi O^-$ ($cm^2\cdot s^{-1}$) | $2.2\cdot10^{-6}$ [c]<br>$0.5\cdot10^{-6}$ [d] | $0.9\cdot10^{-6}$ [c]<br>$0.2\cdot10^{-6}$ [d] |
| Viscosity of water in hydration layer (cP) | 1.6–7 | 3–12 |

[a] Contribution of 0.02 osmol of buffer.
[b] Estimated from the data of Parsegian et al. [77].
[c] Calculated from the rate constant assuming total electrostatic screening by ions within the hydration layer and $R_0 = 6$ Å.
[d] Calculated from the rate constant assuming no electrostatic screening of the interacting ions and $R_0 = 6$ Å.

and decreased in parallel with $d_w$ (compare columns I and II). The viscosity of the water in this microscopic space, deduced from the rate of proton exchange between the pyranin anion and the fixed phospho headgroup on the surface, is very close to that of bulk water, corroborating the findings of Israelashvilli [80].

### *III-E. Geminate recombination within a thin water lamella*

Another method for evaluating the diffusion of protons at the water/phospholipid interface within a very short time frame is to monitor the geminate recombination of a proton with the excited pyranin anion.

When pyranin is trapped in an aqueous lamella, the intensity of $\phi OH^*$ emission is substantially intensified with respect to that measured in bulk water. Application of osmotic pressure further increases this tendency. Two mechanisms contribute to that effect: the lowered activity of water in the lamella delays the dissociation of the proton (see Fig. 3), while the slower diffusion coefficient (see Table II) enhances the probability of geminate recombination (see Fig. 5C).

It must be stressed that the steady-state fluorescence of pyranin is an average of a stroboscopic observation. What we observe are reactions taking place during an approx. 5 ns time window, separating between excitation and decay. Thus, any observed protonation of $\phi O^{*-}$ is by a proton present at an approx. 5 ns diffusion distance (40 Å or less), which is comparable with the width of the aqueous lamella ($d_w$). This allows us to investigate the relative contribution of the two mechanisms discussed at the beginning of this chapter, geometrical constraints vs. slower diffusion of proton in semi-ordered water.

The geminate recombination of $H^+$ and excited pyranin anion was measured in water lamella bounded by DPPC or DPPC + cholesterol at a 1 : 1 molar ratio. The dependence of $d_w$ on the external pressure of these two preparations [78] is quite different; consequently, at a given osmotic pressure (which also sets the $a_{H_2O}$ value) the two types of vesicle will have different $d_w$ spacings. The dominant factor governing geminate recombination will be that one where data points collected with the two preparations will merge into a single population.

The results shown in Fig. 11 clearly demonstrate that the major factor leading to accelerated geminate recombination in thin water layers is the (semi) ordering of water molecules as expressed by $a_{H_2O} < 1$. This corroborates our conjecture that the rapid randomization of the percolating hydrogen-bonded network is a crucial step in proton diffusion.

The ordering of water in hydrophobic cavities [66], as in water channels [81] will not seal it against proton flux, but definitely will slow the rate at which a proton transverses this channel. Any quantitative evaluation of proton flux through structured water must account for the specific conductivity within the site under study.

### *III-F. Inside a proton well*

The proton well was introduced by Peter Mitchell as an element of chemiosmotic machinery that converts $\Delta\psi$ into $\Delta$pH. It is envisioned as a cavity in a membranal protein which almost penetrates the whole width

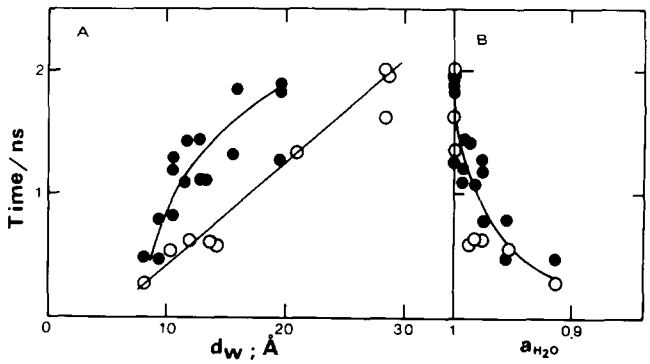


Fig. 11. The dependence of geminate recombination time on the geometry and physical properties of the reaction space. A proton was photodissociated from pyranin trapped within the aqueous lamella in multilamellar liposome made from dimyristoylphosphatidylcholine (●) or its 1 : 1 mixture with cholesterol (○). The recombination dynamics were monitored fluorometrically with a time resolution of 10 ps. The ordinates denote the average geminate recombination time as defined by Eqn. 6. (A) The recombination time related to the width ($d_w$) of the aqueous lamella. The width was adjusted by external osmotic pressure, applied by sucrose. (B) The same parameter related to the activity of the water in the lamella. This value was taken as equal to the activity of the water in the suspending sucrose solution (Rochel, Huppert and Gutman, unpublished results).

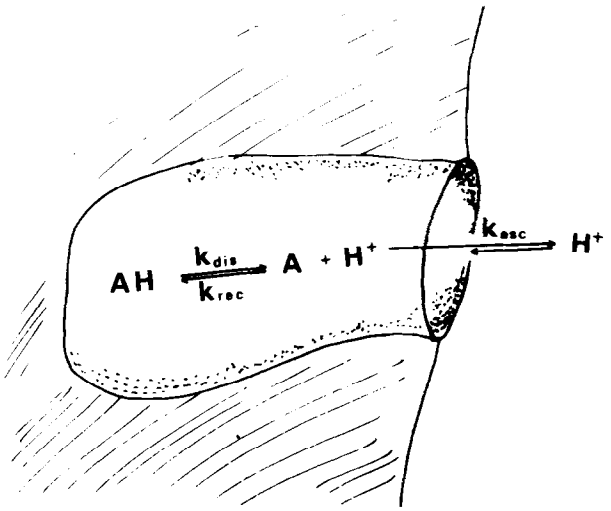


Scheme IV.

of the structure. The high electric field at the bottom of the well attracts protons, so that their concentration within the cavity is larger than in the bulk phase.

Thermodynamically, this scenario is legitimate and viable, yet we must examine also the time element of the mechanism. How long will proton be confined within such a microscopic space? Considering the fact that energy transformation (by conformation changes or via covalent bond formation) proceeds at a finite rate, the dwell time of proton within the well must be, at least, comparable with the time constant of the energy-trapping process.

There is a large similarity between the dynamics of a proton in a proteinaceous cavity and geminate recombination. In both cases, the proton and the site are bound together and interact without being affected by reactants out of the cavity (or the cage). Thus measurements of geminate recombination within a cavity can supply the information about the conditions in the confined space. Obviously the complexity of the reaction within a protein exceeds that of a simple Coulomb cage; for example, the boundaries of the proton well are not spherically symmetric; there is an opening to the bulk and the activity of water in the cavity is less than $a_{H_2O} = 1$.

A general description of the system, suitable for analytic solution, is given in Scheme IV.

A proton from the bulk enters the cavity by a diffusion-controlled reaction and in few nanoseconds reacts with a binding site ($A^-$). At about neutrality the average time interval between proton entries will be about 1 m. Energy-consuming events like ATP synthesis also fall in the millisecond time frame. These two events are much slower than the protonation of $A^-$ or the escape of a proton from the cavity. Thus, our discussion will consider only intracavity proton transfer dynamics and how they modulate the total dwell time of the proton.

Experiments in these directions are based on photodissociation of proton from a pyranin molecule inserted in the heme binding site of apomyoglobin [18] or in hydrophobic sites of bovine serum albumin [13].

The rate constants of the steps defined in Scheme IV are given in Table III, and their magnitude reflects the special intracavity conditions. The rate of dissociation within the site is significantly slower than in bulk water (column 2 of Table III, indicating that the activity of water within a microscopic cavity in a protein is less than 1.

The rate constants of recombination ($k_{rec}$) and escape ($k_{esc}$) are orders of magnitude faster than the entry of proton into cavity or the ensuing catalysis. Thus, the mean probability of finding of a free proton in a protonated well will be determined by the inside reactions, as given by:

$$\frac{[H^+]_{in}}{[AH]} = \frac{k_d}{[A^-]k_{rec} + k_{esc}}$$

The value in the nominator, rate of proton dissociation, is a function of the p$K$ and activity of water in the cavity. For acids with p$K > 4$ (such as carboxylates), its magnitude will be $k_{diss} < 10^6\ s^{-1}$.

The denominator is the sum of two reactions which remove the free proton from the cavity, and allow its escape and binding to $A^-$. $k_{rec}$ is comparable to diffu-

TABLE III

*The rate constant of proton transfer reactions within the haem-binding site of apomyoglobin and pyranin-binding site of bovine serum albumin*

| Protein | $K^a$ ($M^{-1}$) | $k_d$ ($\tau_d$) | $k_{rec}$ ($\tau_{rec}$) | $k_{esc}$ ($\tau_{esc}$) | $a_{H_2O}$ | $\tau_{dwell}$ of $H^+$ |
|---|---|---|---|---|---|---|
| Pyranin free | – | $9 \cdot 10^9$ | – | – | 1.0 | – |
| | | (0.11 ns) | – | – | | |
| Apomyoglobin [b] | $9 \cdot 10^6$ | $6.9 \cdot 10^8$ | $9.3 \cdot 10^8$ | $1.38 \cdot 10^8$ | 0.68 | 1.6 ns |
| | | (1.45 ns) | (1.07 ns) | (7.24 ns) | | |
| Bovine serum albumin [c] | $7 \cdot 10^6$ | $2.2 \cdot 10^9$ | $9.3 \cdot 10^8$ | $1.38 \cdot 10^8$ | 0.8 | 3.7 ns |
| | | (0.45 ns) | (1.07 ns) | (7.7 ns) | | |

[a] The association constant of the dye-protein complex.
[b] Data from Ref. 18.
[c] Data from Ref. 13.

sion controlled reaction times the nominal concentration of $A^-$ in the cavity (about 1 M). $k_{esc}$ is approximated by

$$k_{esc} = \frac{6D}{R^2} \cdot \frac{r}{R}$$

where $R$ and $r$ are the radii of the cavity and opening, respectively, and $D$ is the effective diffusion coefficient within the cavity. Both values $k_{rec}$ and $k_{esc}$ are in the order of $10^9$–$10^{10}$, implying that the probability of finding a free proton in a cavity is extremely small, $10^{-4}$ or less. The sites will either be empty or will retain the proton by a covalent bonding (AH).

To conserve the energy associated with the trapped proton, its lifetime within the cavity must be comparable to the time constant of the energy conversion step. $\tau_{dwell}$, the time frame where the proton is held within the cavity, is given by

$$\tau_{dwell} = \tau_d \left( \frac{k_{rec}}{k_{esc}} + 1 \right)^{-1} \quad (9)$$

As seen in this expression, $\tau_{dwell}$ is first of all proportional to the p$K$ of the proton binding moiety and further modulated by $a_{H_2O}$ within the cavity (Figs. 3 and 4). Secondly, it is modified by the ratio of the intracavity reactions, $k_{rec}/k_{esc}$. When recombination is faster than escape, as in the two cases listed in Table III, the dwell time of the proton will be prolonged.

A long dwell time is a mandatory requirement for proton-coupled reactions where two protons are simultaneously present in the catalytic site [82]. As there is an upper limit for the p$K$ of the proton-trapping moiety in the cavity (it should be lower than the pH of the medium with which it interacts), low activity of water within the cavity and $k_{rec} > k_{esc}$ should be incorporated in the design of the site to make it an effective mechanism.

### *III-G. Ensemble properties of the surface*

With respect to proton's size, the surface of protein (or membrane) is heterogeneous. It is covered by negative electrostatic traps and positive ridges with energies reaching 3–4 $kT$. The local intensive fields are few ånströms in size and when sites are located at 15 Å (or less) apart, they can form a continuum of merged Coulomb cages [54].

A proton attracted to such a surface will propagate by a mechanism corresponding with local forces as applied to each point on the surface. There will be the general trend to escape to the bulk, due to gradient of $a_{H_2O}$ and the impenetrability of the surface. In parallel, the electric fields will bias the diffusion, where the positive ridges either expel it to the bulk, or direct it into the negative valleys. These effects of course dominate only very close to the surface, before the local heterogeneity is blurred into the average charge where the Tanford-Kirkwood [83] equations become applicable. In this section we shall integrate all these factors into comprehensive ensemble description.

The basic experimental system for monitoring an ensemble behaviour is made of inert surface carrying two types of proton binding site, each with known thermodynamic and kinetic constants. The expected observation will be the modulation of one group dynamics by the reactivity of the other. A neutral micelle made of Brij-58 marked with two pH indicators satisfies these demands. One indicator, Bromocresol green, is negatively charged, while the other, Neutral red, is not. Thus the micelle can be loaded with many Neutral red molecules without changing its surface charge [55]. It was observed that the dynamics of reversible protonation of the Bromocresol green was modulated by the number of Neutral red moieties on the micelle. The single proton adsorbed on the mixed micelle was more susceptible for reaction with bulk reactant ($\phi O^-$) when located on the Neutral red ($NRH^+$) rather than on the other indicator ($BCGH^-$). The Neutral red moieties acted as proton-radiating antennae, facilitating the distribution of protons between surface and bulk. The key event which makes this pathway feasible is the rapid exchange of proton between adjacent surface groups. This rate, formally written as collisional proton exchange (but see reservation in subsection II-C.4a) is in the order of $10^{10}$ $M^{-1} \cdot s^{-1}$ [51,59], although even faster rates were already measured [84].

A surface carrying many proton binding sites, like carboxylates of protein or phosphomoieties of phospholipid membrane, can be protonated on any site. The low p$K$ of these groups (p$K \approx 5$ and 2.2, respectively) corresponds with a short lifetime of the bound proton (see Fig. 4), but upon dissociating, it will be captured with high probability by the next one. The probability of the capture is function of the distance between them, thus a denser surface coverage promotes an efficient proton sharing. The whole assembly of temporary binding sites forms a network covering the structure (or regions of it). Through this network, a proton will propagate by a two-dimensional random walk, a strategy which enhances the probability of sampling of any element in the group [19,57,58,79].

A conductive mechanism based on connectivity of the elements is very sensitive to a break in the continuity, as demonstrated experimentally in Fig. 12. Curve A depicts the reversible protonation of fluorescein molecules covalently attached to bovine serum albumin, a reaction which is facilitated by proton transfer through the 100 carboxylates on the protein surface [59]. Random blocking of about 20% of the protein carboxyls suffices to markedly modify the protonation dynamics

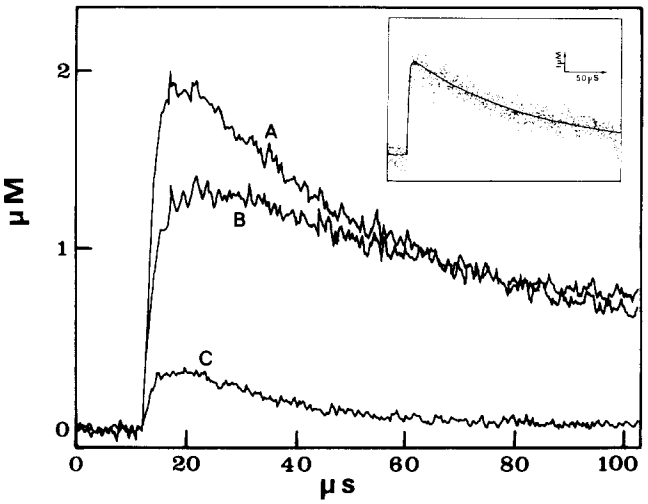


Fig. 12. The effect of random amidation of the carboxylate moieties of bovine serum albumin on the protonation dynamics of the protein-fluorescein adduct. The reaction was initiated by photodissociation of a proton from an emitter in the bulk of the solution, and defecting its reaction with the protein-bound dye. Curve A is of a native protein dye adduct. The smooth curve in the insert is its reconstructed dynamics using rate constants which are listed in Yam et al. [59]. Curves B and C are of the same adduct after random amidation of about 20% and about 45% of the protein carboxylate moieties. The figure is taken from Yam [84].

(compare curves A [unmodified] and B [modified]). More extensive blocking of the carboxylates almost eliminates the protonation (curve C) [85]. Precise numerical analysis of the results [84] indicates that blocking about 20% of the carboxylates lowered the rate of surface proton transfer between $COO^-$ and the dye from $2 \cdot 10^{10}\ M^{-1} \cdot s^{-1}$ to $8 \cdot 10^9$.

The crucial role of proton exchange between surface groups has been established by quantitative analysis of many systems: liposomes [57], black lipid membranes [51], proton-driven $Na^+$ exchange by monensin [86] and various proteins (lysosyme, RNAse and pepsinogen [84]). In all these cases the surface functioned as efficient antenna, collecting/radiating the protons at the bulk surface junction.

The efficiency of the antenna is self-limited in time and space, declining rapidly with the distance covered by proton and its dwell time on the surface. The probability of proton dissociating from one site to be trapped by the nearest one is less than 100%, even merged Coulomb cages cannot prevent the proton from leakage to the bulk. (A hypothetical Coulomb cage 100 Å in size still loses about 50% of its protons within less than 1 ns; see Fig. 5A.) If this is true for a single cage, then nearby sites will also exchange protons with finite probability of losing them to the bulk. Suppose that a merged Coulomb cage made of two sites, 10 Å apart, can retain protons within it with about 90% efficiency. Even in this case, the proton population on the surface will dwindle to $1/e$ within $N = 9$ transfer events. In this example the length constant of the antenna is $d = 10\sqrt{N} = 30$ Å. A transfer of a proton over a longer stretch will be inefficient.

We conclude that the mobility of proton between surface groups is a delicate mechanism calling for continuum of overlapping Coulomb cages. Within these restrictions the network will increase the trapping radius of all protonable groups with subsequent increase in the rate constant of all bulk surface reactions. Thus, it is an efficient mechanism to accelerate the bulk surface equilibration but cannot function as a long-distance proton guide.

## IV. Concluding remarks

In this review we have indicated the general features of proton transfer dynamics with emphasis on proton diffusion as its special case. Propagation of proton in aqueous solution is thus subjected to all forces affecting proton transfer. It is sensitive to local electric fields, water-surface interactions, connectivity of water molecules, geometrical constraints of the reaction space and the presence of other proton binding sites.

The spatial heterogeneity of proteins or a membrane's surface is comparable with the dimension of the space where the environment modulates the rate of proton transfer (a few water molecules in diameter). Thus, the heterogeneity of the surface also implies a nonuniformity of the rate of proton transfer at the interface. At a distance of about 20 Å the local effects fade and a bulk regime is already effective.

Proton transfer reactions, as measured by enzymic catalysis, are macroscopic events compared with the elementary steps we have discussed. Thus, the scenarios proposed to interpret biochemical observations must comply with the microscopic mechanism, not contradict it.

It is our conviction that we have provided in this review the intuitive guidelines suitable for bridging between the microscopic events and the dynamics of biochemical processes.

## Acknowledgements

The authors are grateful to Dr. D. Huppert, Dr. V.A. Parsegian, Z. Ophir, E. Pines, S. Rochel and R. Yam for discussion and communication of results and manuscripts before publication. The research in the Laser Laboratory for Fast Reactions in Biology is supported by the American Israel Binational Science Foundation (Grant No. 87.00235) and the U.S. Navy (Grant No. N00014-89-J-1622).

## References


1 Scheiner, S. (1986) Methods Enzymol. 127, 456–465.
2 Scheiner, S. (1988) J. Mol. Struct. 177, 79–91.
3 Cybulski, S.M. and Scheiner, S. (1989) J. Am. Chem. Soc. 111, 23–31.
4 Scheiner, S., Redfern, P. and Hillenbrand, E.A. (1986) Int. J. Quantum Chem. 29, 817–827.
5 Zundel, G. (1983) in Biophysics (Hoppe, W., Lohman, W., Markl, H. and Zigler, H., eds.), pp. 243–254, Springer, Berlin.
6 Leuchs, H. and Zundel, G. (1982) Can. J. Chem. 60, 2118–2131.
7 Leberle, K., Kempf, I. and Zundel, G. (1989) Biophys. J. 55, 637–648.
8 Schioberg, D. and Zundel, G. (1976) Can. J. Chem. 56, 2193–2200.
9 Nagle, J.F. and Morowitz, H.J. (1978) Proc. Natl. Acad. Sci. USA 75(1), 298–302.
10 Haines, T.H. (1983) Proc. Natl. Acad. Sci. USA 80, 160–164.
11 Brzezinski, B., Zundel, G. and Kramer, R. (1987) J. Phys. Chem. 91, 3077–3080.
12 Warshel, A. (1984) Proc. Natl. Acad. Sci. USA 81, 444–468.
13 Gutman, M., Huppert, D. and Nachliel, E. (1982) Eur. J. Biochem. 121, 637–642.
14 Huppert, D., Kolodney, E., Gutman, M. and Nachliel, E. (1982) J. Am. Chem. Soc. 104, 6949–6953.
15 Bardez, E., Goguillon, B.T., Keh, E. and Valeur, B. (1984) J. Phys. Chem. 88, 1909–1913.
16 Shizuka, H., Ogiwara, T., Narita, A., Sumitani, H. and Yoshihara, K. (1986) J. Phys. Chem. 90, 6708–6714.
17 Politi, M. and Chaimovich, H. (1986) J. Phys. Chem. 90, 282–287.
18 Gutman, M., Nachliel, E. and Hupprt, D. (1982) Eur. J. Biochem. 125, 175–181.
19 Stanley, H.E. and Teixeira, J. (1980) J. Chem. Phys. 73, 3404–3422.
20 Belch, A.C., Rice, S.A. and Sceats, M.G. (1981) Chem. Phys. Lett. 77, 455–459.
21 Careri, G., Geraci, M. and Rupley, J.A. (1985) Proc. Natl. Acad. Sci. USA 82, 5342–5346.
22 Huppert, D. and Kolodney, E. (1981) Chem. Phys. 63, 401–410.
23 Onsager, L. (1973) in Physics and Chemistry of Ice (Walley, E., Jones, S.J., Gold, L.W., eds.), pp. 7–12, Royal Society of Canada.
24 Pines, E. and Huppert, D. (1985) Chem. Phys. Lett. 116, 295–300.
25 Kasianowicz, J., Benz, R. and McLaughlin, S. (1987) J. Membr. Biol. 95, 73–89.
26 Pines, E., Huppert, D., Gutman, M., Nachliel, E. and Fishman, M. (1986) J. Phys. Chem. 90, 6366–6370.
27 Nachliel, E., Ophir, Z. and Gutman, M. (1987) J. Am. Chem. Soc. 109, 1342–1345.
28 Pines, E. and Huppert, D. (1983) J. Phys. Chem. 87, 4471–4478.
29 Gutman, M., Nachliel, E. and Moshiach, S. (1989) Biochemistry 28, 2936–2941.
30 Agmon, N. (1988) J. Chem. Phys. 88, 5639–5642.
31 Wolfbeis, O.S., Furlinger, E., Kroneis, H. and Marsoner, H. (1983) Fresenius Z. Anal. Chem. 314, 119–124.
32 Howitz, K.T. and McCarty, R.E. (1988) Plant Physiol. 86, 999–1001.
33 Kano, K. and Fendler, J.H. (1978) Biochem. Biophys. Acta 509, 289–299.
34 Clement, N.R. and Gould, J.M. (1981) Biochemistry 20, 1534–1538.
35 Pines, E., Huppert, D. and Agmon, N. (1988) J. Chem. Phys. 88, 5620–5630.
36 Agmon, N., Pines, E. and Huppert, D. (1988) J. Chem. Phys. 88, 5631–5638.
37 Weller, A. (1961) Prog. Reaction Kinetics 1, 189–214.
38 Engasser, J.-M. and Horvath, C. (1974) Biochim. Biophys. Acta 358, 178–192.
39 Goldman, R., Kedem, O., Silman, H.T., Kaplan, S.R. and Katchalski, E. (1968) Biochemistry 7, 486–500.
40 Linskog, S. and Coleman, J.E. (1973) Proc. Natl. Acad. Sci. USA 70, 2505–2508.
41 Kara-Ivanov, M. (1983) J. Bioenerg. Biomembr. 15, 111–119.
42 Nunogaki, K. and Kasai, M. (1988) J. Theor. Biol. 134, 403–415.
43 Crank, J. (1979) in The Mathematics of Diffusion, p. 327, Clarendon, London.
44 Junge, W. and McLaughlin, S. (1987) Biochim. Biophys. Acta 890, 1–5.
45 Junge, W. and Polle, A. (1986) Biochim. Biophys. Acta 848, 256–273.
46 Czerlinsky, G.H. (1966) in Chemical Relaxation, Marcel Dekker, New York.
47 Gutman, M. (1986) Methods in Enzymol. 127, 522–538.
48 Gutman, M. (1984) Methods in Biochem. Anal. 30, 1–103.
49 Krishnamoorthy, G. (1986) Biochemistry 25, 6666–6671.
50 Huebner, J.S., Popp, A.E. and Williams, K.R. (1988) J. Chem. Ed. 65, 102–106.
51 Gutman, M., Nachliel, E., Bamberg, E. and Christensen, B. (1987) Biochim. Biophys. Acta 905, 390–398.
52 Marinetti, T. (1987) Biophys. J. 52, 115–122.
53 Ruf, H. and Grell, E. (1981) in Membrane Spectroscopy (Grell, E., ed.), pp. 333–376, Springer-Verlag, Berlin.
54 Matthew, J.B. and Richards, F.M. (1982) Biochemistry 21, 4989–4999.
55 Gutman, M. and Nachliel, E. (1985) Biochemistry 24, 2941–2946.
56 Nachliel, E. and Gutman, M. (1988) J. Am. Chem. Soc. 110, 2629–2635.
57 Adam, G. and Delbruck, M. (1968) in Structural Chemistry and Molecular Biology (Rich, A. and Davidson, N., eds.), pp. 198–215, Freeman, San Francisco.
58 Berg, H.C. and Purcell, E.M. (1977) Biophys. J. 20, 193–219.
59 Yam, R., Nachliel, E. and Gutman, M. (1988) J. Am. Chem. Soc. 110, 2636–2640.
60 Sigolat, C., Haraux, F., De Kouchkovsky, F., Phung Nhu Hung, S. and De Kouchkovsky, Y. (1985) Biochim. Biophys. Acta 809, 403–413.
61 Nalge, J.F. and Dilley, R.A. (1986) J. Bioenerg. Biomembr. 18, 55–64.
62 Theg, S.M., Chiang, G. and Dilley, R.A. (1988) J. Biol. Chem. 263, 673–681.
63 Pick, U. (1988) Biochemistry 27, 8284–8290.
64 Kell, D.B. (1979) Biochim. Biophys. Acta 549, 55–99.
65 Luzar, A., Svetina, S. and Zeks, B. (1985) J. Chem. Phys. 82, 5146–5154.
66 Teeter, M.M. (1984) Proc. Natl. Acad. Sci. USA 81, 6014–6018.
67 Gallay, J., Vincent, M., Nicot, C. and Waks, M. (1987) Biochemistry 26, 5738–5747.
68 Rand, P. and Parsegian, P.A. (1989) Biochim. Biophys. Acta, in press.
69 Israelashvili, J.N. and Mara, J. (1986) Methods Enzymol. 127, 353–360.
70 Robinson, R.A. and Stokes, R.H. (1959) in Electrolyte Solutions, Butterworth, London.
71 Einstein, A. (1906) Ann. Phys. 19, 289.
72 Yam, R., Nachliel, E., Moshiach, S. and Gutman, M. (1989) in Water and Ions in Solution (Vasilescu, V. and Pullman, B., eds.), Birkhauser, in press.
73 Gutman, M., Nachliel, E. and Fishman, M. (1986) in Ion Interactions in Energy Transfer Biomembrane (Papageorgio, G.C., Barber, J. and Papa, S., eds.), pp. 93–104, Plenum, London.
74 Prats, M., Tocanne, J.F. and Teissie, J. (1987) J. Membr. Biol. 99, 225–227.
75 Prats, M., Tocanne, J.F. and Teissie, J. (1987) Eur. J. Biochem. 162, 379–385.
76 Prats, M., Tocanne, J.F. and Teissie, J. (1985) Eur. J. Biochem. 149, 663–668.

77 Kasianowicz, J., Benz, R., Gutman, M. and McLaughlin, S. (1987) J. Membr. Biol. 99, 227.
78 Lis, L.J., McAlister, M., Fuller, N., Rand, R.P. and Parsegian, V.A. (1982) Biophys. J. 37, 657–666.
79 Hardt, S.L. (1979) Biophys. Chem. 10, 239–243.
80 Israelashvili, J.N. (1986) J. Colloid Interface Sci. 110, 263–271.
81 Lear, J.D., Wasserman, Z.R. and DeGrado, W.F. (1988) Science 240, 1177–1181.
82 Gregory-Dewey, T. and Hammes, G.G. (1981) J. Biol. Chem. 256, 8941–8946.
83 Tanford, C. and Kirkwood, J.G. (1957) J. Am. Chem. Soc. 79, 5333–5339.
84 Yam, R. (1990) Ph.D. Thesis, Tel Aviv University, Israel.
85 Yam, R. (1988) in The Ion Pumps: Structures, Function and Regulation (Stein, W.D., ed.), pp. 279–282, Alan R. Liss, New York.
86 Gutman, M. and Nachliel, E. (1990) Electrochem. Acta, in press.